**RESEARCH ARTICLE**

## Developmental Genetics of Corolla Tube Formation: Role of the tasiRNA-*ARF* Pathway and a Conceptual Model

Baoqing Ding, [a,1] Rui Xia,[b,c] Qiaoshan Lin,[a] Vandana Gurung,[a] Janelle M. Sagawa,[a] Lauren E. Stanley,[a] Matthew Strobel,[a] Pamela K. Diggle,[a] Blake C. Meyers,[c,d] Yao-Wu Yuan[a,e,1]

[a]Department of Ecology and Evolutionary Biology, University of Connecticut, Storrs, CT 06269, USA
[b]State Key Laboratory for Conservation and Utilization of Subtropical Agro-Bioresources, South China Agricultural University, Guangzhou, Guangdong 510642, China
[c]Donald Danforth Plant Science Center, St. Louis, MO 63132, USA
[d]Division of Plant Sciences, University of Missouri–Columbia, Columbia, MO 65211, USA
[e]Institute for Systems Genomics, University of Connecticut, Storrs 06269, USA

[1]Corresponding authors:
Baoqing Ding (ding.baoqing@gmail.com); Yao-Wu Yuan (yuan.colreeze@gmail.com)

**Short title:** Genetic control of corolla tube formation

**One-sentence summary:** We show that the tasiRNA-*ARF* pathway is required for corolla tube formation in monkeyflowers (*Mimulus*) and propose a new conceptual model highlighting the central role of auxin-directed synchronized growth in congenital petal fusion.

The author responsible for distribution of materials integral to the findings presented in this article in accordance with the policy described in the Instructions for Authors (www.plantcell.org) is: Yao-Wu Yuan (yuan.colreeze@gmail.com).

**ABSTRACT**

Over 80,000 angiosperm species produce flowers with petals fused into a corolla tube. The corolla tube contributes to the tremendous diversity of flower morphology and plays a critical role in plant reproduction; yet it remains one of the least understood plant structures from a developmental genetics perspective. Through mutant analyses and transgenic experiments, we show that the tasiRNA-*ARF* pathway is required for corolla tube formation in the monkeyflower species *Mimulus lewisii*. Loss-of-function mutations in the *M. lewisii* orthologs of *ARGONAUTE7* and *SUPPRESSOR OF GENE SILENCING 3* cause a dramatic decrease in abundance of *TAS3*-derived small RNAs and a moderate up-regulation of *AUXIN RESPONSE FACTOR 3* (*ARF3*) and *ARF4*, which lead to inhibition of lateral expansion of the bases of petal primordia and complete arrest of the upward growth of the inter-primordial regions, resulting in unfused corollas. Using the *DR5* auxin responsive promoter, we discovered that auxin signaling is continuous along the petal primordium base and the inter-primordial region during the critical stage of corolla tube formation in the wild-type, similar to the spatial pattern of Ml*ARF4* expression. Auxin response is also much weaker and more restricted in the mutant. Furthermore, exogenous application of polar auxin transport inhibitor to wild-type floral apices disrupted petal fusion. Together, these results suggest a new conceptual model highlighting the central role of auxin-directed synchronized growth of the petal primordium base and the inter-primordial region in corolla tube formation.

**INTRODUCTION**

About one third of the ~275,000 angiosperm species produce flowers with petals fused into a corolla tube (i.e., sympetalous), forming a protective enclosure around nectaries and reproductive organs. Corolla tubes have evolved multiple times independently across the angiosperm tree of life (Endress, 2011), most notably in the common ancestor of the Asterids, a clade containing more than 80,000 species (Schonenberger and Von Balthazar, 2013). Subsequent elaboration in length, width, and curvature has led to a great variety in corolla tube shapes that enabled asterid species to exploit many specialized pollinator groups (e.g., bee flies, hawkmoths, hummingbirds, nectar bats), which in turn drives rapid plant speciation (Muchhala, 2006; Hermann and Kuhlemeier, 2011; Paudel et al., 2015; Lagomarsino et al., 2016). As such, the corolla tube has long been considered a key morphological innovation that contributed to the radiation of the Asterids (Endress, 2011). Despite its critical importance in the reproductive success and evolution of such a large number of species, the corolla tube remains one of the least understood plant structures from a developmental genetics perspective (Specht and Howarth, 2015; Zhong and Preston, 2015; Rebocho et al., 2017; Preston et al., 2019).

Historically, corolla tube formation has been the subject of extensive morphological and anatomical studies (Boke, 1948; Kaplan, 1968; Govil, 1972; Nishino, 1976, 1978, 1983a, 1983b; Erbar, 1991; Erbar and Leins, 1996; Kajita and Nishino, 2009; El Ottra et al., 2013). In particular, numerous studies have described the detailed ontogenetic process of corolla tube development in one subgroup of the asterid clade, the Lamiids, which contains some classical plant genetic model systems such as snapdragon (*Antirrhinum*), petunia (*Petunia*), and morning glory (*Ipomoea*) (Govil, 1972; Nishino, 1976, 1978, 1983a, 1983b; Singh and Jain, 1979; Erbar, 1991; Vincent and Coen, 2004; Kajita and Nishino, 2009; Erbar and Leins, 2011). A common theme emerging from these studies is that during the early stage of petal development, petal primordia are initiated separately, followed by rapid extension of the petal bases toward the inter-primordial regions, which also grow coordinately, causing congenital fusion of the petal primordia and formation of the corolla tube. Little is known, however, about the genetic control of this early-phase lateral extension of the petal base or the nature of this coordinated inter-primordial growth.

A handful of genes have been implicated in corolla tube formation. Loss-of-function mutations in *FEATHERED* (*FE*) in Japanese morning glory (*Ipomoea nil*) and *MAEWEST*

(*MAW*) in petunia (*Petunia x hybrida*), both generated by transposon insertions, result in unfused corollas (Iwasaki and Nitasaka, 2006; Vandenbussche et al., 2009). *FE* and *MAW* encode KANADI and WOX transcription factors, and their Arabidopsis (*Arabidopsis thaliana*) orthologs are *KANADI1* and *WOX1*, respectively. In addition, ectopic accumulation of Arabidopsis TEOSINTE BRANCHED 1, CYCLOIDEA AND PCF TRANSCRIPTION FACTOR 5 (TCP5) fused with a repressor motif in *Ipomoea* disrupted corolla tube formation (Ono et al., 2012). However, whether the endogenous *TCP5* ortholog in *Ipomoea* is involved in corolla tube development is unclear. It was also reported that transient knock-down of the petunia genes encoding the NAC-transcription factors NO APICAL MERISTEM (NAM) and NAM-like protein 16 (NH16) by virus-induced gene silencing (VIGS) caused decreased petal fusion (Zhong et al., 2016). However, the interpretation of this result was confounded by the observation that occasional flowers produced on escape shoots of the loss-of-function *nam* mutants had normal corolla tubes (Souer et al., 1996). In addition, *NAM* expression was not detected between petal boundaries in petunia (Preston et al., 2019). The fact that these genes were characterized from different plant systems and through different methods (transposon insertion alleles, heterologous expression of a chimeric repressor, and VIGS) makes it challenging to interpret their genetic relationships and their precise functional roles in corolla tube formation.

One solution around this problem is to systematically analyze corolla tube mutants in a single model system. To this end, we employ a new genetic model system, the monkeyflower species *Mimulus lewisii*, mainly for its relative ease of use in chemical mutagenesis and Agrobacterium (*Agrobacterium tumefaciens*)-mediated in planta transformation (Owen and Bradshaw, 2011; Yuan et al., 2013a; Yuan, 2019). *M. lewisii* is a typical bumblebee-pollinated species with a conspicuous corolla tube (Figure 1A). Through ethyl methanesulfonate (EMS) mutagenesis, we have generated a dozen recessive mutants (named *flayed*) with unfused corollas. Here we report the characterization of one group of mutants, caused by loss-of-function mutations in two genes that are required for the biogenesis of *trans*-acting short interfering RNAs (tasiRNAs).

Among the tasiRNA loci characterized to date, *TRANS-ACTING SIRNA3* (*TAS3*) is the most widely conserved, found in virtually all land plants (Xia et al., 2017). *TAS3* transcripts bear two binding sites for microRNA390 (miR390), which triggers the production of phased

tasiRNAs, including the highly conserved "tasiARF" that targets *AUXIN RESPONSE FACTOR 2* (*ARF2*), *ARF3*, and *ARF4* transcripts (Allen et al., 2005; Williams et al., 2005; Axtell et al., 2006). The tasiRNA-*ARF3/4* regulatory module plays a critical role in leaf adaxial/abaxial polarity and blade expansion (i.e., lamina growth) in both eudicots (Fahlgren et al., 2006; Garcia et al., 2006; Hunter et al., 2006; Yan et al., 2010; Yifhar et al., 2012; Zhou et al., 2013) and monocots (Nagasaki et al., 2007; Nogueira et al., 2007; Douglas et al., 2010). Consistent with previous studies, here we demonstrate that in the *M. lewisii* mutants, *TAS3*-derived tasiRNAs decrease dramatically in abundance and that Ml*ARF3* and Ml*ARF4* expression are upregulated. Importantly, we show that malfunction of the tasiRNA-*ARF* pathway in *M. lewisii* mutants impedes the early lateral expansion of the petal primordium bases and their coordinated inter-primordial growth, most likely through a change in auxin homeostasis, leading to unfused petal primordia. Integrating our molecular and phenotypic analyses of the tasiRNA-*ARF* pathway and the spatial patterns of Ml*ARF4* expression and auxin responses in *M. lewisii* with historical insights from morphological and anatomical studies of various sympetalous species, we propose a new conceptual model for the genetic control of corolla tube formation. This model offers logical connections among the previous sporadic reports of corolla tube mutants and makes clear predictions that can be readily tested using the *Mimulus* system.


## RESULTS

### Phenotypic Characterization of the *flayed1* and *flayed2* Mutants

The recessive mutants *flayed1-flayed3* recovered from EMS mutagenesis using the inbred line LF10 were morphologically indistinguishable. Pair-wise crosses suggested that they belong to two complementation groups, *flayed1* and *flayed2* (*flayed3* being allelic to *flayed2*) (Figures 1B and 1C). In addition to having unfused petals, these mutants displayed carpel fusion defects, with phenotypes varying from flower to flower within the same plant. Most mutant flowers had two fused carpels, as in the wild type, but with partially split stigmas with more than two lobes (Figure 1E), while some flowers had two almost completely separate styles. The length of mutant pistils was also reduced compared to the wild type (Figure 1E). No obvious phenotypes were observed in the stamens of these mutants.

Another notable feature of the *flayed1/2* mutants was the reduced width of their lateral organs. The dorsal and lateral petals showed ~30% decrease in width compared to the wild type, and ~37% decrease for the ventral petal (Figure 1F; Supplemental Table 1). The mutations also substantially reduced leaf width by ~40%, but length remained unaffected (Figures 1G and 1H; Supplemental Table 1). To determine whether the reduction in petal width was due to changes in cell number, cell size, or both, we measured the width of abaxial (outer) epidermal cells of the dorsal petal lobe for both wild-type and *flayed2* flowers. Because petal lobe abaxial epidermal cells are irregularly shaped (Figure 1I), we performed width measurements on five contiguous cells to account for the variation among individual cells within the same sample. We detected no significant differences in cell width between the wild type and *flayed2* (Figure 1J), suggesting that the difference in petal width between the mutant and the wild type is primarily due to a difference in cell number (i.e., number of cell divisions).

Unlike the morning glory *fe* mutant (Iwasaki and Nitasaka, 2006) or the petunia *maw* mutant (Vandenbussche et al., 2009), *flayed1/2* mutants did not show any defects in tissue adaxial/abaxial polarity. Instead, the *flayed1/2* mutants closely resembled the petunia mutant *choripetala suzanne* (*chsu*), which also exhibits unfused corollas, variable carpel fusion defects, and narrower leaves with normal adaxial/abaxial polarity. Unfortunately, the molecular identity of *CHSU* is still unknown.

### *FLAYED1* and *FLAYED2* Are the Orthologs of Arabidopsis *AGO7* and *SGS3*, Respectively

To identify the causal genes behind the *flayed1* and *flayed2* mutants, we analyzed each mutant using a genomic approach that combines the advantages of bulk-segregant analysis and comparison of single nucleotide polymorphism (SNP) profiles between multiple EMS mutants (**Methods**), as demonstrated in a previous study (LaFountain et al., 2017). We narrowed down the causal mutations for *flayed1* and *flayed2* to 38 and 19 candidate SNPs, respectively (Supplemental Tables 2 and 3). The vast majority of these SNPs located in non-coding, repetitive sequences, with only two or three mutations resulting in amino acid changes in each mutant (Supplemental Tables 2 and 3). Notably, each mutant showed a single point mutation leading to a premature stop codon, in the ortholog of Arabidopsis *ARGONAUTE7* (*AGO7*) for *flayed1* and in *SUPPRESSOR OF GENE SILENCING 3* (*SGS3*) for *flayed2* (Figures 2A and 2B; Supplemental Tables 2 and 3). *AGO7* and *SGS3* are part of the same tasiRNA biogenesis

pathway (Peragine et al., 2004; Yoshikawa et al., 2005; Chen, 2010), which would explain the identical phenotypes exhibited by *flayed1* and *flayed2*. Furthermore, sequencing the coding sequence (CDS) of Ml*SGS3* in *flayed3*, which is allelic to *flayed2*, revealed an independent mutation that also led to a premature stop codon (Figure 2B). Together, these results suggested that Ml*AGO7* and Ml*SGS3* were the most promising candidate genes for *FLAYED1* and *FLAYED2*.

To validate these gene identities, we introduced the full-length CDS for Ml*AGO7* and Ml*SGS3* into the *flayed1* and *flayed2* mutant background, respectively, driven by the cauliflower mosaic virus *35S* promoter (CaMV 35S). Among 29 independent *35Spro:*Ml*AGO7* lines in the *flayed1* background, 13 showed a fully rescued phenotype that was indistinguishable from the wild type; four lines showed partial rescue, with petal and leaf width similar to that of the wild type but with unfused petals (Figure 2C). Similarly, six of the 18 Ml*SGS3* over-expression lines in the *flayed2* background displayed a fully rescued phenotype and two exhibited partial rescue (Figure 2D). RT-qPCR assessment of Ml*AGO7* and Ml*SGS3* expression in 5 mm floral buds showed that expression levels of the transgenes were 4~64-fold higher than those of the corresponding endogenous genes in the fully rescued lines (Figures 2E and 2F). These results confirmed that Ml*AGO7* and Ml*SGS3* were indeed the causal genes underlying *flayed1* and *flayed2*.

Knowing the causal genes and mutations also allowed direct genotyping of a "*flayed1* x *flayed2*" F2 population to identify *flayed1 flayed2* double mutants, which were phenotypically indistinguishable from the single mutants (Figures 1D and 1F to 1H). This result further indicated that Ml*AGO7* and Ml*SGS3* functioned in the same genetic pathway in *Mimulus*, as expected.

**The *flayed1/2* Phenotypes Are Primarily Mediated Through the tasiRNA-*ARF* Pathway**

*AGO7* and *SGS3* are necessary components of the miR390-*TAS3-ARF* pathway (Figure 3A), and the highly conserved, *TAS3*-derived tasiARFs are known to play a critical role in leaf polarity and lamina growth by repressing *ARF3/4* expression. We therefore hypothesized that the *flayed1/2* phenotypes (e.g., reduced width of lateral organs) were primarily mediated through the tasiRNA-*ARF* pathway. Three clear predictions derive from this hypothesis: (**i**) the abundance of *TAS3*-derived small RNAs, including tasiARFs, should be much lower in the mutants compared

to the wild type; (**ii**) the *M. lewisii ARF3/ 4* orthologs should be upregulated in the mutants; and, (**iii**) artificial up-regulation of the *M. lewisii ARF3/4* orthologs in the wild-type background should recapitulate the *flayed1/2* phenotypes. We chose to focus on *ARF3/4* rather than *ARF2*, the other known target of tasiARFs (Williams et al., 2005; Marin et al., 2010), because most of the traits controlled by *ARF2* in Arabidopsis (e.g., seed size, leaf senescence, floral organ abscission, fruit ripening and dehiscence; Ellis et al., 2005; Okushima et al., 2005; Schruff et al., 2006; Lim et al., 2010) were unaffected in our *flayed1/2* mutants compared to the wild type.

To test the first prediction, we sequenced the total small RNA pool from young floral buds (5 mm) from the wild type and the *flayed1* and *flayed 2* mutants. Like most other angiosperms, *M. lewisii* had two kinds of *TAS3* genes (each represented by only a single copy in the *M. lewisii* genome): *TAS3S* contained a single, centrally located tasiARF, whereas *TAS3L* contained two tandem tasiARFs (Xia et al., 2017) (Supplemental Figure 1). We detected no *TAS3S*-derived small RNAs in any of the sequenced samples, suggesting that the *TAS3S* gene was not expressed. By contrast, we detected *TAS3L*-derived small RNAs to the level of ~600 per million reads in the wild type, but these decreased >50-fold in both *flayed1* and *flayed2* (Figure 3B). In particular, tasiARFs were almost entirely absent from the mutant samples (Figure 3B). These results validated the first prediction.

To test the second prediction, we first searched the *M. lewisii* genome for *ARF3/4* homologs and identified a single putative ortholog for each gene. Similar to *ARF3/4* in other species, both Ml*ARF3* and Ml*ARF4* had two binding sites with sequences complementary to tasiARF (Figures 4A and 4B). RT-qPCR measurements in 5 mm floral buds showed that Ml*ARF3* was up-regulated by 1.7~2.5-fold and Ml*ARF4* was up-regulated by 2.7~3.7-fold in the single and double mutants (Figure 4C). This moderate upregulation of *ARF3/ARF4* in the *ago7* and *sgs3* mutant backgrounds was very similar to previous reports in Arabidopsis (Garcia et al., 2006; Hunter et al., 2006), supporting the role of tasiARF in fine-tuning *ARF3/4* expression levels.

To test the third prediction, we transformed the wild type with a tasiARF-insensitive version of Ml*ARF3* (*m*Ml*ARF3*) and Ml*ARF4* (*m*Ml*ARF4*) with several synonymous substitutions in the tasiARF binding sites (Figures 4A and 4B), driven by the 35S promoter. We obtained seven independent *35Spro:m*Ml*ARF3* and 14 *35Spro:m*Ml*ARF4* lines. In each case, only two transgenic lines showed obvious phenotypes: their leaves were very similar to the

*flayed1/2* mutants (i.e., narrower than the wild type) with partially split corollas (indicated by the red arrowheads in Figures 4D and 4E). RT-qPCR experiments on 5 mm floral buds of the transgenic lines with even the strongest phenotypes showed only moderate overexpression of Ml*ARF3/4* relative to the wild type (2~4-fold, Figures 4G and 4H). Examination of two random *35Spro:mMlARF4* lines without obvious phenotypes showed no increase in Ml*ARF4* expression levels (Figure 4I). The lack of *35Spro:m*Ml*ARF3/4* lines with strong transgene expression contrasted with the ectopic expression of Ml*AGO7* and Ml*SGS3* (Figures 2E and 2F) as well as that of pigment-related transcription factors in *M. lewisii* (Yuan et al., 2014; Sagawa et al., 2016; Ding et al., 2020), where the same 35S promoter readily drove transgene expression levels >10-fold higher than the endogenous genes. One possible explanation for this observation is that transgenic lines with very strong *ARF3/4* expression in *M. lewisii* are seedling-lethal, as implicated by similar experiments in tomato (*Solanum lycopersicum*) (Yifhar et al., 2012). Nevertheless, our results showed that a moderate upregulation of Ml*ARF3/4* indeed fully recapitulated the leaf phenotype and partially recapitulated the flower phenotype of the *flayed1/2* mutants. Furthermore, a double transgenic line derived from a cross between the strongest *35Spro:m*Ml*ARF3* line and *35Spro:m*Ml*ARF4* line showed dramatic petal fusion defects (Figure 4F), indicating that Ml*ARF3* and Ml*ARF4* may act synergistically in regulating corolla tube formation. Taken together, our results from transgenic manipulation of the Ml*ARF3/4* expression levels suggested that the *flayed1/2* phenotypes (narrow leaf and unfused corollas) were primarily mediated by the upregulation of Ml*ARF3/4*.

**The tasiRNA-*ARF* Pathway is Required for Preferential Lateral Expansion of the Bases of Petal Primordia and Coordinated Growth of Inter-primordial Regions**

To understand how malfunction of the tasiRNA-*ARF* pathway affects corolla tube formation in *M. lewisii*, we studied floral organogenesis in the wild type and the *flayed2* mutant using scanning electron microscopy. Like other species in the lamiid clade (e.g., snapdragon, petunia, morning glory), *M. lewisii* petals initiated as five separate primordia (Figure 5A). Petal development lagged behind stamens in the early stages (Figures 5B and 5C), but by the time the corolla reached 0.5 mm in diameter (Figure 5D), petal development progressed rapidly and soon the stamens were enclosed in the corolla (Figures 5E to 5H). The developmental stage from 0.3 to 0.4 mm (corolla diameter) was critical for corolla tube formation: during this stage, the bases

of the petal primordia quickly expanded laterally (to a conspicuously greater extent than the upper portion of the petal primordia; Figure 5M), and the inter-primordial regions also grew coordinately, connecting the initially separate petal primordia. Floral organogenesis of *flayed2* was very similar to that of the wild type during the early stages (before the corolla reaches 0.3 mm in diameter; Figure 5I). However, during the critical period (0.3~0.4 mm), we observed no preferential lateral expansion at the bases of the petal primordia in the mutant, manifested as the truncate shape of the petal primordium base (Figure 5N), in contrast to the semi-circle shape seen in the wild type (Figure 5M). Notably, growth of the inter-primordial regions was also arrested in *flayed2*, leading to a gap between two adjacent petal primordia (Figures 5J to 5L and indicated by the asterisk in Figure 5N).

Given that disruption of tasiRNA biogenesis and the consequent upregulation of *ARF3/4* have been shown to cause reduced lamina growth of lateral organs in multiple plant species (Peragine et al., 2004; Douglas et al., 2010; Yan et al., 2010; Yifhar et al., 2012; Zhou et al., 2013), it was perhaps not surprising to observe reduced lateral expansion at the bases of petal primordia in *flayed2* compared to the wild type (Figures 5M and 5N). But how does this observation explain the arrest of upward growth of the inter-primordial regions?

In a series of careful anatomical studies of various taxa in the Asterids, Nishino recognized that the co-operation between the marginal meristem activities at the base of the petal primordia and the upward growth of the inter-primordial regions played a pivotal role in corolla tube formation (Nishino, 1976, 1978, 1983a, 1983b), although the nature of this co-operation has been unclear. Considering this earlier insight, together with our own results (Figures 5M and 5N), we speculated that in the wild type, there was a molecular signal with continuous distribution in the marginal meristematic cells along the petal primordium base and the inter-primordial region, stimulating synchronized growth between the two regions. In the *flayed2* mutant, this growth signal may be reduced or disrupted in its spatial distribution, leading to arrested growth in the zone encompassing the margins of primordium base and the inter-primordial region. An obvious candidate for this putative signal would be the phytohormone auxin, which is known to promote localized tissue outgrowth while also suppressing the expression of organ boundary genes such as *CUP-SHAPED COTYLEDON 1* (*CUC1*) and *CUC2* in Arabidopsis (Bilsborough et al., 2011).

**Spatial Distribution of Auxin Response in Developing Corolla Buds Corresponds to Petal Growth Patterns in the Wild Type and Auxin Homeostasis is Altered in *flayed2***

To examine the spatial pattern of auxin responses in developing corollas, we introduced the auxin response reporter construct *DR5rev:mRFPer* (Gallavotti et al., 2008), driving the expression of the red fluorescent protein (RFP) by the synthetic auxin-responsive promoter *DR5*, into the wild type LF10. In the very early stage when petal primordia have just initiated (corresponding to a stage between Figures 5A and 5B), we detected strong RFP signal in both petal primordia and inter-primordial regions, with a clear gap between the two (Figure 6A). As the corolla reached 0.4 mm in diameter, RFP signal became concentrated at the apex of the petal primordium and the "synchronized growth zone" encompassing the margins along the primordium base and the inter-primordial region (between the arrowheads in Figure 6B), with relatively weaker signal along the upper part of the petal primordium margin. It is worth noting that the spatial pattern of auxin response at this stage corresponded almost perfectly with the petal growth pattern leading to corolla tube formation (i.e., preferential lateral expansion of the petal primordium base and the coordinated upward growth of the inter-primordial region; Figure 5M). As the corolla reached 0.5 mm in diameter, auxin responses remained continuous at the base of the petal primordium and the inter-primordial region (demarcated by the arrow heads in Figure 6C), but the gap devoid of auxin response between the petal apex and the synchronized growth zone became more conspicuous than at the 0.4 mm stage. When the corolla reached 0.6 mm in diameter, RFP signal started to spread more evenly along the entire petal margin (Figure 6D), likely corresponding to later growth of the entire corolla. While all confocal images shown in Figure 6 were taken using *DR5rev:mRFPer* line 2, examination of several additional independent transgenic lines showed very similar results.

To test whether auxin homeostasis was altered in the *flayed2* mutant, we crossed *DR5rev:mRFPer* line 2 with *flayed2*, and analyzed $F_2$ individuals homozygous for the *flayed2* mutation and with the *DR5rev:mRFPer* transgene. When imaged under the same microscopy parameters, *flayed2* corollas showed much weaker RFP signal overall than the wild type (Figures 6E and 6F). In particular, the junction between the petal primordium base and the inter-primordial region (arrows in Figures 6E and 6F) showed no RFP signal at all, consistent with the lack of synchronized growth between these two regions in the mutant (Figure 5N). The relatively

weak RFP signal in the mutant pistil (Figures 6E and 6F) also correlated with the split stigma/style phenotype (Figure 1E).

**Exogenous Application of Polar Auxin Transport Inhibitor Disrupts Corolla Tube Formation**

If auxin was indeed the signaling molecule that stimulated synchronized growth between the petal primordium base and the inter-primordial region, exogenous application of polar auxin transport inhibitors during the early stages of corolla development may disrupt the spatial pattern of auxin signaling and thereby interfere with corolla tube formation. To test this prediction, we treated wild-type lateral shoot apices with 1-N-naphthylphthalamic acid (NPA) using a "spray/vacuum infiltration" approach (see Methods for details). About 30% of the ~250 flowers that opened 3-to-4 weeks after the NPA treatment showed various defects in corolla tube formation (Figure 7A), whereas none of the ~250 flowers produced by mock-treated plants showed any obvious phenotypic alterations. Reciprocally, exogenous application of the auxin indole-3-acetic acid (IAA) to *flayed2* lateral shoot apices resulted in the rescue of corolla tube formation in five of the ~250 flowers (Figure 7B), whereas none of the flowers on the mock-treated plants showed any phenotypic rescue. This relatively low frequency (2%) of corolla tube rescue by IAA treatment in the mutant, compared to the moderate frequency (30%) of corolla tube disruption by NPA treatment in the wild type, was not unexpected, as it is much easier to destroy the delicate spatial pattern of auxin signaling than to restore it by exogenous applications of the corresponding chemicals.

**Ml*ARF4* Expression Coincides with the Spatial Pattern of Auxin Response in the Developing Corolla**

To further investigate how the tasiRNA-*ARF* pathway may relate to the spatial patterning of auxin signaling in the developing corolla, we studied the spatial expression pattern of Ml*ARF4*. We focused on Ml*ARF4* because it was functionally redundant with Ml*ARF3* in corolla tube formation (Figures 4D to 4F), its transcript levels were higher than Ml*ARF3* in wild-type floral buds based on unpublished transcriptome data, and its expression levels were up-regulated to a higher degree than Ml*ARF3* in the *flayed1/2* mutants (Figure 4C). We transformed the wild type LF10 with the reporter construct Ml*ARF4pro:*Ml*ARF4-RFP*, which contains a ~8-kbp Ml*ARF4*

genomic DNA fragment (~3-kbp promoter sequence upstream of the translation initiation site plus all exons and introns), with *RFP* cloned at the 3' end. A careful examination of individual petals in multiple Ml*ARF4pro:*Ml*ARF4-RFP* transgenic lines showed that Ml*ARF4* predominantly localized to the abaxial side of the developing petal (Figures 8A and 8B), resembling the *ARF3/4* expression pattern in leaf primordia of Arabidopsis and tomato (Yifhar et al., 2012; Guan et al., 2017). More importantly, the Ml*ARF4* expression pattern in the young corollas was very similar to the spatial pattern of auxin response. When the corolla was 0.5 mm in diameter, Ml*ARF4* was concentrated in the synchronized growth zone (i.e., the inter-primordial region and the adjacent primordium bases) (Figure 8C), similar to the pattern of auxin response at the same developmental stage (Figure 6C). In 0.6 mm corollas, Ml*ARF4* expression became more widespread along the petal margin (Figure 8D), reminiscent of the *DR5:RFP* signals observed earlier (Figure 6D).

This coincidence of the Ml*ARF4* expression pattern and *DR5:RFP* signal in the synchronized growth zone provided a plausible explanation for the reduced auxin response in the *flayed2* mutant. *Ml*ARF3/4 can repress auxin responses through at least two non-exclusive mechanisms: (**i**) ARF3/4 are known to repress auxin signaling by competing with ARF activators (e.g., ARF5/6/7/8) for the auxin response element (AuxRE) binding sites in the promoters of auxin-responsive genes (Tiwari et al., 2003; Vernoux et al., 2011; Lavy et al., 2016); (**ii**) ARF3 has been shown to directly repress auxin biosynthesis and transport in Arabidopsis (Simonini et al., 2017). Therefore, upregulation of Ml*ARF3/4* in the *flayed2* mutant would be expected to exert stronger repression of auxin signaling in the synchronized growth zone, leading to arrested growth and lack of corolla tube formation.

It should be noted that there was also an obvious difference between the Ml*ARF4pro:*Ml*ARF4-RFP* signal and the *DR5:RFP* signal: the former was not found at the apex of the petal primordium, although the latter was (Figures 6C and 8C). This difference indicated that *Ml*ARF3/4 were not the only regulators of auxin signaling in the developing corolla.

**DISCUSSION**

This study represents the first step in a systematic effort towards understanding the developmental genetics of corolla tube formation using the new model system *Mimulus lewisii*. We showed here that the tasiRNA-*ARF* pathway is required for synchronized growth between the petal primordium base and the inter-primordial region at early stages of corolla development. Furthermore, we discovered that auxin signaling is continuous in this synchronized growth zone in the wild type, similar to the spatial pattern of Ml*ARF4* expression. Upregulation of Ml*ARF3/4* in the *flayed2* mutant correlated with much reduced auxin response in the synchronized growth zone, explaining the inhibition of lateral expansion at the base of the petal primordia and complete arrest of the upward growth of the inter-primordial regions observed in the mutant. Together, these results suggest a new conceptual model for the developmental genetic control of corolla tube formation, highlighting the central role of auxin signaling in the synchronized growth zone.

**Role of the tasiRNA-*ARF* Pathway in Petal Fusion**

Although this is the first detailed study investigating the role of the tasiRNA-*ARF* pathway in corolla tube formation, a previous study on leaf development in the family Solanaceae has mentioned in passing that malfunction of the tasiRNA-*ARF* pathway led to unfused corollas in tomato and tobacco (*Nicotiana tabacum*) flowers (Yifhar et al., 2012). Like *Mimulus*, the family Solanaceae belongs to the asterid clade. This suggests that the role of the tasiRNA-*ARF* pathway in corolla tube formation is likely conserved across asterid plants. More surprisingly, two other studies of leaf development in barrelclover (*Medicago truncatula*) and trefoil (*Lotus japonicus*), both belonging to the legume family (Fabaceae), also implicated an indispensable role for the tasiRNA-*ARF* pathway in petal fusion (Yan et al., 2010; Zhou et al., 2013). Typical legume flowers have separate dorsal and lateral petals, but the two ventral petals often fuse into a prow-shaped structure (i.e., the "keel"). In the *ago7* mutants of *M. truncatula* and *L. japonicus*, the two ventral petals become separated. The family Fabaceae belongs to the clade Rosids. Given that the vast majority of rosid species (e.g., Arabidopsis) produce flowers with completely separate petals (i.e., polypetalous), with only a few exceptions in derived lineages (Zhong and Preston, 2015), it is clear that the tasiRNA-*ARF* pathway was independently recruited to enable petal fusion in the legume species.

There are two significant insights emerging from our molecular and phenotypic analyses of the tasiRNA-*ARF* pathway in *Mimulus* that were not known from the aforementioned studies that focused on leaf development: (**i**) the tasiRNA-*ARF* pathway is required not only for the lamina growth of petal primordia, but also for the upward growth of the inter-primordial regions (Figures 5M and 5N). In fact, we think that the synchronized growth between the petal primordium base and the inter-primordial region is the key to corolla tube formation; (**ii**) there is a tight correlation between the spatial pattern of Ml*ARF4* expression, auxin response, and the growth of the inter-primordial region in developing corollas (Figure 5M; Figures 6B and 6C; Figure 8C), establishing a mechanistic link between the tasiRNA-*ARF* pathway, auxin signaling, and corolla tube formation.

The difference in spatial patterns of auxin response between *flayed2* and the wild type (Figure 6) suggested that the role of the tasiRNA-*ARF* pathway in corolla tube formation may lie in the regulation of auxin homeostasis. Indeed, the coincidence of the Ml*ARF4* expression pattern and the spatial pattern of auxin response suggests that Ml*ARF3/4* play an important role in modulating the level of auxin signaling in the synchronized growth zone. In Arabidopsis, loss-of-function *arf3* mutations displayed increased *DR5:GFP* signal in the gynoecium (Simonini et al., 2017). Conversely, upregulation of *ARF3/4* homologs in the moss species *Physcomitrium patens*, either due to loss of *SGS3* function or transgenic overexpression, resulted in decreased auxin response (Plavskin et al., 2016; Lavy et al., 2016). These observations suggest that ARF3/4 and their homologs can clearly function as negative regulators of auxin response, at least in some developmental contexts. Indeed, recent studies have shown that these repressive ARFs can negatively regulate auxin response by competing with activating ARFs for the same AuxRE binding sites in the promoters of auxin-responsive genes (Lavy et al., 2016), or directly repressing the transcription of auxin biosynthesis and transport genes via histone deacetylation (Simonini et al., 2017; Chung et al., 2019; Kuhn et al., 2020). Similar to the synchronized growth zone in the developing *M. lewisii* corolla**,** overlaps between the spatial pattern of *ARF3/4* expression and auxin response also have been shown in lateral root primordia (Marin et al., 2010), founder cells of the reproductive primordia (Vernoux et al., 2011; Chung et al., 2019), and the abaxial side of leaf primordia (Guan et al., 2017) in Arabidopsis. These patterns suggest that in most developmental contexts, ARF3/4 do not act as a simple "off" switch to auxin response. Instead, they are usually part of a more complex genetic regulatory network with

negative feedback loops that fine-tune local auxin responses (Marin et al., 2010; Vernoux et al., 2011; Plavskin et al., 2016). Since tasiARF small RNAs are a key component of these negative feedback loops (Marin et al., 2010; Plavskin et al., 2016), their complete depletion in the *flayed2* mutant (Figure 3B) is expected to disrupt the robustness of the feedback regulation and explains the reduced level of auxin response in *flayed2* (Figures 6E and 6F). The specific configuration of the auxin response genetic regulatory network in the developing corollas of sympetalous species like *Mimulus lewisii* warrants further investigation.

**Relationship between Petal Lamina Growth and Corolla Tube Formation**

Given the well-known function of the tasiRNA-*ARF* pathway in lamina growth of lateral organs (Fahlgren et al., 2006; Garcia et al., 2006; Hunter et al., 2006; Nagasaki et al., 2007; Nogueira et al., 2007; Douglas et al., 2010Yan et al., 2010; Yifhar et al., 2012; Zhou et al., 2013) and the reduced petal width of the *flayed1/2* mutants, it is easy to over-interpret the significance of lamina growth of the petal primordia in the "fusion" of adjacent petals. However, the following observations suggest that lamina growth of the petal primordia per se is not the key to corolla tube formation: (**i**) In some of *35Spro:*Ml*AGO7* and *35Spro:*Ml*SGS3* transgenic lines (in the corresponding mutant background), petal width was restored to wild-type levels, but the petals remained unfused (Figures 2C and 2D). In addition, we have several other yet-to-be-characterized *flayed* mutants with unfused corollas but normal petal width. These observations suggest that petal lamina growth at the wild-type level is not sufficient for tube formation; (**ii**) petal width of a previously characterized *M. lewisii* mutant, the dominant-negative actin mutant *act1-D*, is very similar to that of *flayed1/2* (Ding et al., 2017), but the corolla tube of *act1-D* is intact. This suggests that reduced petal lamina growth does not necessarily affect petal fusion. Instead, we think it is the synchronization between the lateral expansion of the petal primordium base and the upward growth of the inter-primordia region, most likely directed by auxin signaling, that holds the key to corolla tube formation.

**A New Conceptual Model for the Developmental Genetic Control of Corolla Tube Formation**

Two recent attempts to build a conceptual framework for floral organ fusion in general (Specht and Howarth, 2015) or petal fusion in particular (Zhong and Preston, 2015) both emphasized the

genetic regulatory network underlying organ boundary formation and maintenance. The rationale for such emphasis was explicitly stated by Specht and Howarth (Specht and Howarth, 2015): "*fusion as a process may more accurately be defined as a lack of organ separation*". While these attempts represent an important step towards a mechanistic understanding of the developmental process of corolla tube formation, to some degree they have neglected the insight provided by earlier morphological and anatomical studies (i.e., the importance of the co-operation between the rapid lateral expansion of the petal primordium base and the upward growth of the inter-primordial region), and have not provided a logical explanation to the previously reported corolla tube mutants (e.g., morning glory *fe*, petunia *maw*) (Iwasaki and Nitasaka, 2006; Vandenbussche et al., 2009) in terms of organ boundary formation or maintenance. Overemphasis on the "lack of organ separation" may represent an underestimation of the complexity of the corolla tube formation process, with the implication that simple loss-of-function mutations in some organ boundary genes in polypetalous species (e.g., Arabidopsis) could produce a functional corolla tube. Despite extensive mutagenesis of Arabidopsis in the past 40 years, such a mutant has not been reported.

Integrating our results on the tasiRNA-*ARF* pathway and the spatial pattern of auxin signaling in *M. lewisii* with previous reports of corolla tube mutants (Iwasaki and Nitasaka, 2006; Vandenbussche et al., 2009) as well as historical insights from anatomical studies (Nishino, 1978, 1983a, 1983b), we propose a new conceptual model for the developmental genetic control of corolla tube formation (Figure 9). At the heart of the model is auxin-induced synchronized growth of the marginal meristematic cells at the base of the petal primordia and the inter-primordial cells, providing a molecular explanation for the co-operation between the petal primordium base and the inter-primordial region observed in anatomical studies. Upstream of this core module is the genetic regulatory network controlling adaxial/abaxial polarity and lamina growth of lateral organs (Nakata and Okada, 2013; Tsukaya, 2013; Kuhlemeier and Timmermans, 2016), which is conserved in a wide range of angiosperms and is somehow co-opted in sympetalous species to regulate auxin homeostasis in the synchronized growth zone. Downstream of this core module lies the genetic network responsible for localized tissue growth induced by auxin signaling.

This model can readily explain the phenotypes of loss-of-function mutations in morning glory *FE* and petunia *MAW*, which encode KANADI and WOX transcription factors,

respectively (Iwasaki and Nitasaka, 2006; Vandenbussche et al., 2009). Together with the tasiRNA-ARF pathway, these transcription factors are part of the genetic network regulating leaf adaxial-abaxial polarity and lamina growth (Nakata and Okada, 2013; Tsukaya, 2013; Kuhlemeier and Timmermans, 2016). Recent studies in other model systems such as Arabidopsis, barrelclover, and tobacco, have demonstrated that these polarity regulators largely function by modulating auxin homeostasis (Tadege et al., 2011; Huang et al., 2014; Simonini et al., 2017). According to our model, interfering with this genetic regulatory network is expected to reduce or disrupt the continuous auxin response in the synchronized growth zone, as shown in the *flayed2* mutant (Figure 5N; Figures 6E and 6F), and consequently resulting in unfused corolla. Our model also provides a plausible explanation for the petal fusion defects observed when a chimeric repressor of Arabidopsis TCP5 was over-expressed in the Japanese morning glory (Ono et al., 2012). Chimeric repressors of CIN-like TCP transcription factors (e.g., Arabidopsis TCP3/4/5) are known to decrease *AGO7* and *TAS3* expression in Arabidopsis (Koyama et al., 2010), which would be expected to upregulate *ARF3/4* and inhibit corolla tube formation in sympetalous species.

One unresolved issue is whether organ boundary genes, such as the homologs of *CUC/NAM*, play an important role in corolla tube formation, as previously proposed (Specht and Howarth, 2015; Zhong and Preston, 2015). A recent observation in snapdragon (Rebocho et al., 2017) appears to support this proposition — the expression of the *CUC/NAM* ortholog, *CUPULIFORMIS (CUP)*, is cleared from the inter-primordial regions shortly after petal initiation but later is reactivated in the sinuses between adjacent corolla lobes. Computational modeling suggested that this "gap" of *CUP* expression (between the base of the corolla and the sinuses) is necessary for corolla tube formation (Rebocho et al., 2017), presumably by releasing the repression of localized tissue growth in the synchronized growth zone. However, if the role of *CUC*-like genes is to repress tissue growth at the petal-petal junction, down-regulation or loss-of-function of *NAM/CUP* should increase the degree of petal fusion. Instead, VIGS-knockdown of *NAM* and its paralog *NH16* in the sympetalous petunia caused decreased petal fusion (Zhong et al., 2016). Furthermore, in situ hybridizations of *NAM* in petunia flowers detected no expression at all in petal-petal boundaries, arguing against a critical role of *NAM* in defining petal-petal boundaries in petunia (Preston et al., 2019). The exact cause of these conflicting

observations is unclear; perhaps future experiments involving ectopic expression of *CUC*-like genes in sympetalous flowers will shed light on this problem.

Given the central role of auxin-directed synchronized tissue growth in corolla tube formation, our model predicts that in addition to the leaf polarity/lamina growth network, disturbance of other genetic pathways that regulate auxin biosynthesis, polar transport, and signaling within and between petal primordia, in transgenic or mutant plants of sympetalous species could also result in defective corolla tubes. The availability of multiple corolla tube mutants, the ease of bulk-segregant analysis to identify mutant genes, and the amenability of Agrobacterium-mediated in planta transformation make *Mimulus* a favorable system to test these predictions and to dissect the detailed molecular mechanisms and developmental process of corolla tube formation.

## METHODS

### Plant Materials and Growth Conditions

We performed EMS mutagenesis on the *Mimulus lewisii* Pursh inbred line LF10, as described (Owen and Bradshaw, 2011). We used the inbred line SL9 to generate *flayed* $F_2$ mapping populations. We grew all plants on FAFARD soil mix #2 (Sun Gro Horticulture) in the University of Connecticut research greenhouses, under natural light supplemented with sodium vapor lamps, ensuring a 16 h daylength and a light intensity of 110-160 $\mu mol \cdot m_{-2} \cdot s_{-1}$.

### Phenotypic Characterization

To quantify phenotypic differences between the mutants and the wild type, we measured the widths of the dorsal, ventral, and lateral petals using a digital caliper. We also measured the lengths and widths of the fourth leaf (the largest leaf) of mature plants. To further evaluate whether the width difference is due to changes in cell number, cell size or both, we measured the width of the abaxial epidermal cells of the dorsal petal lobe following a previously described procedure (Ding et al., 2017).

**Genomic Analyses for Causal Gene Identification**

To identify the causal genes underlying *flayed1* and *flayed2*, we employed a hybrid strategy that combines the advantages of bulk-segregant analysis and genome comparisons between multiple EMS mutants, as described previously (LaFountain et al., 2017). Briefly, we produced an $F_2$ population for each mutant by crossing the homozygous mutant (generated in the LF10 background) to the polymorphic inbred line SL9. We pooled DNA samples from 96 $F_2$ segregants displaying the mutant phenotype (i.e., homozygous for the causal mutation) with equal representation. We then prepared a small-insert library for the pooled sample before sequencing on an Illumina HiSeq 2000 platform at the University of North Carolina High Throughput Sequencing Facility. We generated about 213 and 448 million 100-bp paired-end reads for *flayed1* and *flayed2*, respectively.

We mapped the short reads to the LF10 genome assembly version 1.8 (http://monkeyflower.uconn.edu/resources/) using CLC Genomics Workbench 7.0 (Qiagen, Valencia, CA). The causal mutation should be: (**i**) homozygous in the pooled sample (i.e., 100% SNP frequency in the "$F_2$ reads – LF10 genome" alignment); and (**ii**) unique to each mutant (i.e., any shared 100% SNPs between mutants are most likely due to assembly error in the reference genome, non-specific mapping of repetitive sequences, or private SNPs in our laboratory LF10 stock). After comparisons to the SNP profiles of previously published mutants, *guideless* (Yuan et al., 2013b), *rcp1* (Sagawa et al., 2016), *act1-D* (Ding et al., 2017), and *rcp2* (Stanley et al., 2020), we narrowed the causal mutation to 39 and 19 candidate SNPs for *flayed1* and *flayed2*, respectively (Supplemental Figure 2; Supplemental Tables 2 and 3).

**Small RNA Sequencing and Analyses**

For small RNA sequencing, we extracted total RNA using the Spectrum Plant Total RNA Kit (Sigma-Aldrich) from 5 mm floral buds of LF10, *flayed1*, and *flayed2* (two biological replicates for each genotype). We then constructed small RNA libraries using Illumina TruSeq Small RNA Sample Preparation Kits, with 1 μg of total RNA as starting material. We sequenced the libraries on an Illumina HiSeq 2500 platform at the Delaware Biotechnology Institute (Newark, DE). Small RNA reads were quality-controlled and adaptor-trimmed before calculating tasiRNA abundance, as described in Xia et al. (2017).

**Quantitative RT-PCR**

We performed RNA extraction and cDNA synthesis as previously described (Yuan et al., 2013a). We diluted cDNA samples 10-fold before RT-qPCR. All RT-qPCR reactions were performed using iQ SYBR Green Supermix (Bio-Rad) and a CFX96 Touch Real-Time PCR Detection System (Bio-Rad). Samples were amplified for 40 cycles of 95ºC for 15 s and 60ºC for 30 s. Amplification efficiencies for each primer pair were determined using critical threshold values obtained from a dilution series (1:4, 1:8, 1:16, 1:32) of pooled cDNAs. The *M. lewisii* ortholog of the Arabidopsis ubiquitin-conjugating enzyme gene *At5g25760/UBC21*, Ml*UBC* , was used as a reference gene, as described (Yuan et al., 2013a). Relative expression of each target gene compared to the reference gene was calculated using the formula $(E_{ref})^{CP(ref)} / (E_{target})^{CP(target)}$. Primers used for RT-qPCR are listed in Supplemental Table 4.

**Plasmid Construction and Plant Transformation**

To generate the *35Spro:MlAGO7* and *35Spro:MlSGS3* constructs for rescue experiments, we PCR-amplified the full-length CDS of Ml*AGO7* and Ml*SGS3* from wild-type LF10 cDNAs using the Phusion enzyme (NEB, Ipswich, MA). For each gene, we cloned the amplified fragment into the pENTR/D-TOPO vector (Invitrogen) before using it as a template to amplify a linear fragment containing the CDS flanked by the attL1 and attL2 sites using M13 primers. We then recombined this linear fragment into the Gateway vector pEarleyGate 100 (Earley et al., 2006), which drives transgene expression from the CaMV *35S* promoter. To generate the *35Spro:mMlARF3/4* constructs, we synthesized the CDS of sRNA insensitive forms for Ml*ARF3* (*m*Ml*ARF3*) and Ml*ARF4* (*m*Ml*ARF4*) with synonymous substitutions in the two tasiRNA recognition sites at GenScript (Piscataway, NJ) and before cloning into the pEarleyGate 100 destination vector as described for the *35Spro:MlAGO7* and *35Spro:MlSGS3* constructs. To generate the *ARF4pro:ARF4-RFP* reporter construct, we cloned a ~8-kbp genomic fragment for Ml*ARF4* , including the ~3-kbp promoter sequence upstream of the translation starting site and all exons and introns, into the pDONOR207 vector before recombination into the pGWB653 destination vector (Nakamura et al., 2010). All plasmids were verified by sequencing before being transformed into Agrobacterium (*Agrobacterium tumefaciens*) strain GV3101 for subsequent plant transformation, as described in Yuan et al. (2013a). Primers used for plasmid construction and sequencing are listed in Supplemental Table 5.

## Scanning Electron Microscopy

We fixed flower buds overnight in Formalin-Acetic-Alcohol (FAA) at 4ºC, dehydrated for 30 min through a 50%, 60%, 70%, 95%, and 100% ethanol series. Samples were then critical-point dried, mounted, and sputter-coated before observation using a NOVA NanoSEM with Oxford EDX at 35 kV at UConn's Bioscience Electron Microscopy Laboratory.

## Confocal Microscopy

We observed early developing floral buds (with sepals removed if necessary) carrying the *DR5rev:mRFPer* construct by laser confocal microscopy in the red channel as Z-stacks. All fluorescence images were acquired at UConn's Advanced Light Microscopy Facility using a Nikon A1R confocal laser scanning microscope equipped with a 20x/0.45 S Plan Fluor ELWD objective lens with the shoot apex temporarily under water. For the *DR5:RFP* reporter lines, all imaging was done using the same confocal settings, with a laser line of 558 nm, pinhole size of 46 μm, and laser power of 15. For the *ARF4pro:ARF4-RFP* reporter lines, imaging was done with a laser line of 558 nm, pinhole size of 56 μm, and laser power of 21.

## NPA and IAA treatments

To prepare plants for NPA and IAA treatments, we pinched the shoot apex of seedlings at the eight-leaf stage (i.e., four pairs of leaves) to promote lateral growth. Once each plant produced at least a dozen lateral shoots, we sprayed the apex of each lateral shoot with 5 μM NPA in 0.2% DMSO (for the wild type) or 5 mM IAA in water (for the *flayed2* mutants) using a mist bottle. We then placed the plants in a vacuum chamber and applied a pressure of 15 in Hg for 2 min before being released quickly. Each treatment was applied to five plants with corresponding mock treatment controls (i.e., 0.2% DMSO solution or water was applied to wild-type and *flayed2* plants, respectively)

## Accession Numbers

Short read data have been deposited in NCBI SRA (BioProject PRJNA423263); small RNA data have been deposited in NCBI GEO (GSE108530); annotated gene sequences have been deposited in GenBank: Ml*AGO7* (MG669632), Ml*SGS3* (MG669633), Ml*ARF4* (MG669634)

and Ml*ARF3* (MF084285); Ml*UBC* sequence is available from Mimubase (http://mimubase.org/) under accession number ML6G280000.

**Supplemental Data**

**Supplemental Figure 1.** Annotation of the *TAS3* transcripts in *Mimulus lewisii*.

**Supplemental Figure 2.** SNP profile comparison between different EMS mutants.

**Supplemental Table 1.** Phenotypic measurements of the wild-type, *flayed1*, *flayed2*, and the double mutant.

**Supplemental Table 2.** *flayed1* Candidate SNPs.

**Supplemental Table 3.** *flayed2* Candidate SNPs.

**Supplemental Table 4.** Primers used for RT-qPCR.

**Supplemental Table 5.** Primers used for plasmid construction and sequence verification.

**Supplemental Data Set 1.** Summary of statistical tests.

**AUTHOR CONTRIBUTIONS**

Y.W.Y. conceived the project. B.D. and Y.W.Y. designed the research. B.D., R.X., Q.L., V.G., J.M.S., L.E.S., M.S., and P.K.D. performed the experiments. B.D., Y.W.Y., P.K.D., R.X., and B.C.M. analyzed data. B.D. and Y.W.Y. wrote the manuscript with input from all the authors.

## REFERENCES

**Allen, E., Xie, Z., Gustafson, A.M., Carrington, J.C.** 2005. microRNA-directed phasing during trans-acting siRNA biogenesis in plants. Cell **121**: 207-221.

**Axtell, M.J., Jan, C., Rajagopalan, R., and Bartel, D.P.** (2006). A two-hit trigger for siRNA biogenesis in plants. Cell **127:** 565-577.

**Bilsborough, G.D., Runions, A., Barkoulas, M., Jenkins, H.W., Hasson, A., Galinha, C., Laufs, P., Hay, A., Prusinkiewicz, P., Tsiantis, M.** 2011. Model for the regulation of *Arabidopsis thaliana* leaf margin development. Proc. Natl. Acad. Sci. USA **108:** 3424-3429.

**Boke, N.H.** (1948). Development of the perianth in *Vinca rosea* L. Am. J. Bot. **35**: 413-423.

**Chen, X.** (2010). Small RNAs - secrets and surprises of the genome. Plant J. **61**: 941-958.

**Chung, Y., Zhu, Y., Wu, M.-F., Simonini, S., Kuhn, A., Armenta-Medina, A., Jin, R., Østergaard, L., Gillmor, C.S., and Wagner, D.** (2019). Auxin response factors promote organogenesis by chromatin-mediated repression of the pluripotency gene *SHOOTMERISTEMLESS*. Nature communications **10**: 1-11.

**Ding, B., Mou, F., Sun, W., Chen, S., Peng, F., Bradshaw, H.D., and Yuan, Y.-W.** (2017). A dominant-negative actin mutation alters corolla tube width and pollinator visitation in *Mimulus lewisii*. New Phytol. **213**: 1936-1944.

**Ding, B., Patterson, E.L., Holalu, S.V., Li, J., Johnson, G.A., Stanley, L.E., Greenlee, A.B., Peng, F., Bradshaw Jr, H., and Blinov, M.L.** (2020). Two myb proteins in a self-organizing activator-inhibitor system produce spotted pigmentation patterns. Curr. Biol. **30**: 802-814.

**Douglas, R.N., Wiley, D., Sarkar, A., Springer, N., Timmermans, M.C., and Scanlon, M.J.** (2010). *ragged seedling2* encodes an ARGONAUTE7-like protein required for mediolateral expansion, but not dorsiventrality, of maize leaves. Plant Cell **22**: 1441-1451.

**Earley, K.W., Haag, J.R., Pontes, O., Opper, K., Juehne, T., Song, K.M., and Pikaard, C.S.** (2006). Gateway-compatible vectors for plant functional genomics and proteomics. Plant J. **45**: 616-629.

**El Ottra, J.H.L., Pirani, J.R., and Endress, P.K.** (2013). Fusion within and between whorls of floral organs in *Galipeinae* (Rutaceae): structural features and evolutionary implications. Ann. Bot. **111**: 821-837.

**Ellis, C.M., Nagpal, P., Young, J.C., Hagen, G., Guilfoyle, T.J., and Reed, J.W.** (2005). *AUXIN RESPONSE FACTOR1* and *AUXIN RESPONSE FACTOR2* regulate senescence and floral organ abscission in *Arabidopsis thaliana*. Development **132**: 4563-4574.

**Endress, P.K.** (2011). Evolutionary diversification of the flowers in angiosperms. Am. J. Bot. **98**: 370-396.

**Erbar, C.** (1991). Sympetaly—a systematic character. Bot. Jahrb. Syst. **112**: 417-451.

**Erbar, C., and Leins, P.** (1996). Distribution of the character states "early sympetaly" and "late sympetaly" within the "Sympetalae Tetracyclicae" and presumably allied groups. Plant Biol. **109**: 427-440.

**Erbar, C., and Leins, P.** (2011). Synopsis of some important, non-DNA character states in the asterids with special reference to sympetaly. Bot. Jahrb. Syst. **129**: 93-123.

**Fahlgren, N., Montgomery, T.A., Howell, M.D., Allen, E., Dvorak, S.K., Alexander, A.L., and Carrington, J.C.** (2006). Regulation of *AUXIN RESPONSE FACTOR3* by TAS3 ta-siRNA affects developmental timing and patterning in *Arabidopsis*. Curr. Biol. **16**: 939-944.

**Gallavotti, A., Yang, Y., Schmidt, R.J., and Jackson, D.** (2008). The Relationship between auxin transport and maize branching. Plant Physiol. **147**: 1913-1923.

**Garcia, D., Collier, S.A., Byrne, M.E., and Martienssen, R.A.** (2006). Specification of leaf polarity in *Arabidopsis* via the trans-acting siRNA pathway. Curr. Biol. **16**: 933-938.

**Govil, C.** (1972). Morphological studies in the family convolvulaceae. P. Indian Acad. Sci. B **75**: 271-282.

**Guan, C., Wu, B., Yu, T., Wang, Q., Krogan, N.T., Liu, X., and Jiao, Y.** (2017). Spatial auxin signaling controls leaf flattening in *Arabidopsis*. Curr. Biol. **27**: 2940-2950.

**Hermann, K., and Kuhlemeier, C.** (2011). The genetic architecture of natural variation in flower morphology. Curr. Opin. Plant Biol. **14**: 60-65.

**Huang, T., Harrar, Y., Lin, C., Reinhart, B., Newell, N.R., Talavera-Rauh, F., Hokin, S.A., Barton, M.K., and Kerstetter, R.A.** (2014). Arabidopsis KANADI1 acts as a transcriptional repressor by interacting with a specific cis-element and regulates auxin

biosynthesis, transport, and signaling in opposition to HD-ZIPIII Factors. Plant Cell **26**: 246-262.

**Hunter, C., Willmann, M.R., Wu, G., Yoshikawa, M., de la Luz Gutierrez-Nava, M., and Poethig, S.R.** (2006). Trans-acting siRNA-mediated repression of *ETTIN* and *ARF4* regulates heteroblasty in *Arabidopsis*. Development **133**: 2973-2981.

**Iwasaki, M., and Nitasaka, E.** (2006). The *FEATHERED* gene is required for polarity establishment in lateral organs especially flowers of the Japanese morning glory (*Ipomoea nil*). Plant Mol. Biol. **62**: 913-925.

**Kajita, Y., and Nishino, E.** (2009). Development of leaves and flowers in the wild-type and pleiotropic *maple-willow* mutant of Japanese morning glory (*Ipomoea nil*). J. Jpn. Soc. Hortic. Sci. **78**: 469-477.

**Kaplan, D.R.** (1968). Structure and development of the perianth in *Downingia bacigalupii*. Am. J. Bot. **55**: 406-420.

**Koyama, T., Mitsuda, N., Seki, M., Shinozaki, K., and Ohme-Takagi, M.** (2010). TCP transcription factors regulate the activities of ASYMMETRIC LEAVES1 and miR164, as well as the auxin response, during differentiation of leaves in Arabidopsis. The Plant Cell **22**: 3574-3588.

**Kuhlemeier, C., and Timmermans, M.C.P.** (2016). The Sussex signal: insights into leaf dorsiventrality. Development **143:** 3230-3237.

**Kuhn, A., Harborough, S.R., McLaughlin, H.M., Natarajan, B., Verstraeten, I., Friml, J., Kepinski, S., and Østergaard, L.** (2020). Direct ETTIN-auxin interaction controls chromatin states in gynoecium development. Elife **9**: e51787.

**LaFountain, A.M., Chen, W., Sun, W., Chen, S., Frank, H.A., Ding, B., Yuan, Y-W.** (2017). Molecular basis of overdominance at a flower color locus. G3: Genes, Genomes, Genetics **7**: 3947-3954.

**Lagomarsino, L.P., Condamine, F.L., Antonelli, A., Mulch, A., and Davis, C.C.** (2016). The abiotic and biotic drivers of rapid diversification in Andean bellflowers (Campanulaceae). New Phytol. **210**: 1430-1442.

**Lavy, M., Prigge, M.J., Tao, S., Shain, S., Kuo, A., Kirchsteiger, K., and Estelle, M.** (2016). Constitutive auxin response in Physcomitrella reveals complex interactions between Aux/IAA and ARF proteins. Elife **5**: e13325.

**Lim, P.O., Lee, I.C., Kim, J., Kim, H.J., Ryu, J.S., Woo, H.R., and Nam, H.G.** (2010). Auxin response factor 2 (ARF2) plays a major role in regulating auxin-mediated leaf longevity. J. Exp. Bot. **61**: 1419-1430.

**Marin, E., Jouannet, V., Herz, A., Lokerse, A.S., Weijers, D., Vaucheret, H., Nussaume, L., Crespi, M.D., and Maizel, A.** (2010). miR390, Arabidopsis TAS3 tasiRNAs, and their *AUXIN RESPONSE FACTOR* targets define an autoregulatory network quantitatively regulating lateral root growth. Plant Cell **22**: 1104-1117.

**Muchhala, N.** (2006). Nectar bat stows huge tongue in its rib cage. Nature **444**: 701-702.

**Nagasaki, H., Itoh, J.-I., Hayashi, K., Hibara, K.-I., Satoh-Nagasawa, N., Nosaka, M., Mukouhata, M., Ashikari, M., Kitano, H., and Matsuoka, M.** (2007). The small interfering RNA production pathway is required for shoot meristem initiation in rice. Proc. Natl. Acad. Sci. USA **104**:14867-14871.

**Nakamura, S., Mano, S., Tanaka, Y., Ohnishi, M., Nakamori, C., Araki, M., Niwa, T., Nishimura, M., Kaminaka, H., and Nakagawa, T.** (2010). Gateway binary vectors with the bialaphos resistance gene, bar, as a selection marker for plant transformation. Biosci. Biotech. Bioch **74**: 1315-1319.

**Nakata, M., and Okada, K.** (2013). The leaf adaxial-abaxial boundary and lamina growth. Plants **2**: 174-202.

**Nishino E.** (1976). Developmental anatomy of foliage leaves, bracts, calyx and corolla in *Pharbitis nil*. Bot. Mag. **89:** 191-209.

**Nishino, E.** (1978). Corolla tube formation in four species of Solanaceae. Bot. Mag. **91**:263-277.

**Nishino, E.** (1983a). Corolla tube formation in the Primulaceae and Ericales. Bot. Mag. **96**:319-342.

**Nishino, E.** (1983b). Corolla tube formation in the Tubiflorae and Gentianales. Bot. Mag. **96**:223-243.

**Nogueira, F.T., Madi, S., Chitwood, D.H., Juarez, M.T., and Timmermans, M.C.** (2007). Two small regulatory RNAs establish opposing fates of a developmental axis. Genes Dev. **21**:750-755.

**Okushima, Y., Mitina, I., Quach, H.L., and Theologis, A.** (2005). AUXIN RESPONSE FACTOR 2 (ARF2): a pleiotropic developmental regulator. Plant J. **43**: 29-46.

**Ono, M., Hiyama, S., Higuchi, Y., Kamada, H., Nitasaka, E., Koyama, T., Mitsuda, N., Ohme-Takagi, M., and Sage-Ono, K.** (2012). Morphological changes in *Ipomoea nil* using chimeric repressors of *Arabidopsis* TCP3 and TCP5. Plant Biotechnol. **29**:457-463.

**Owen CR, Bradshaw HD.** (2011). Induced mutations affecting pollinator choice in *Mimulus lewisii* (Phrymaceae). Arthropod Plant Interact. **5**: 235-244.

**Paudel, B.R., Shrestha, M., Dyer, A.G., Zhu, X.-F., Abdusalam, A., and Li, Q.-J.** (2015). Out of Africa: evidence of the obligate mutualism between long corolla tubed plant and long-tongued fly in the Himalayas. Ecol. Evol. **5**:5240-5251.

**Peragine, A., Yoshikawa, M., Wu, G., Albrecht, H.L., Poethig, R.S.** (2004). SGS3 and SGS2/SDE1/RDR6 are required for juvenile development and the production of trans-acting siRNAs in Arabidopsis. Genes Dev. **18:** 2368-2379.

**Plavskin, Y., Nagashima, A., Perroud, P.-F., Hasebe, M., Quatrano, R.S., Atwal, G.S., and Timmermans, M.C.** (2016). Ancient trans-acting siRNAs confer robustness and sensitivity onto the auxin response. Developmental Cell **36**: 276-289.

**Preston, J.C., Powers, B., Kostyun, J.L., Driscoll, H., Zhang, F., and Zhong, J.** (2019). Implications of region-specific gene expression for development of the partially fused petunia corolla. Plant J. **100**: 158-175.

**Rebocho, A.B., Kennaway, J.R., Bangham, J.A., and Coen, E.** (2017). Formation and shaping of the *Antirrhinum* flower through modulation of the *CUP* boundary gene. Curr. Biol. **27**:2610-2622.

**Sagawa, J.M., Stanley, L.E., LaFountain, A.M., Frank, H.A., Liu, C., and Yuan, Y.-W.** (2016). An R2R3-MYB transcription factor regulates carotenoid pigmentation in *Mimulus lewisii* flowers. New Phytol. **209**:1049-1057.

**Schonenberger, J., and Von Balthazar, M.** (2013). Asterids. Bot. J. Linnean Soc. **173**:321-324.

**Schruff, M.C., Spielman, M., Tiwari, S., Adams, S., Fenby, N., and Scott, R.J.** (2006). The *AUXIN RESPONSE FACTOR 2* gene of *Arabidopsis* links auxin signalling, cell division, and the size of seeds and other organs. Development **133**: 251-261.

**Simonini, S., Bencivenga, S., Trick, M., and Ostergaard, L.** (2017). Auxin-induced modulation of ETTIN activity orchestrates gene expression in Arabidopsis. Plant Cell **29**: 1864-1882.

**Singh, V., Jain, D.K.** (1978). Floral organogenesis in *Antirrhinum majus*. P. Indian Acad. Sci. B **3**: 183-188.

**Souer, E., van Houwelingen, A., Kloos, D., Mol, J., Koes, R.** (1996). The no apical meristem gene of *Petunia* is required for pattern formation in embryos and flowers and is expressed at meristem and primordia boundaries. Cell **85**: 159-170.

**Specht, C.D., and Howarth, D.G.** (2015). Adaptation in flower form: a comparative evodevo approach. New Phytol. **206**:74-90.

**Stanley, L.E., Ding, B., Sun, W., Mou, F., Hill, C., Chen, S., Yuan, Y.W.** (2017). A tetratricopeptide repeat protein regulates carotenoid biosynthesis and chromoplast development in monkeyflowers (*Mimulus*). Plant Cell **32**: 1536-1555.

**Tadege, M., Lin, H., Bedair, M., Berbel, A., Wen, J., Rojas, C.M., Niu, L., Tang, Y., Sumner, L., Ratet, P., et al.** (2011). *STENOFOLIA* regulates blade outgrowth and leaf vascular patterning in *Medicago truncatula* and *Nicotiana sylvestris*. Plant Cell **23**:2125-2142.

**Tiwari, S.B., Hagen, G., and Guilfoyle, T.** (2003). The roles of auxin response factor domains in auxin-responsive transcription. Plant Cell **15**: 533-543.

**Tsukaya, H.** (2013). Leaf development. The Arabidopsis Book **11**:e0163.

**Vandenbussche, M., Horstman, A., Zethof, J., Koes, R., Rijpkema, A.S., and Gerats, T.** (2009). Differential recruitment of WOX transcription factors for lateral development and organ fusion in *Petunia* and *Arabidopsis*. Plant Cell **21**:2269-2283.

**Verbeke, J.** (1992). Fusion events during floral morphogenesis. Annu. Rev. Plant Physiol. Plant Molec. Biol. **43**:583-598.

**Vernoux, T., Brunoud, G., Farcot, E., Morin, V., Van den Daele, H., Legrand, J., Oliva, M., Das, P., Larrieu, A., and Wells, D.** (2011). The auxin signalling network translates dynamic input into robust patterning at the shoot apex. Molecular Systems Biology **7**: 508.

**Vincent, C.A., and Coen, E.S.** (2004). A temporal and morphological framework for flower development in *Antirrhinum majus*. Can. J. Bot. **82**:681-690.

**Williams, L., Carles, C.C., Osmont, K.S., and Fletcher, J.C.** (2005). A database analysis method identifies an endogenous trans-acting short-interfering RNA that targets the Arabidopsis *ARF2*, *ARF3*, and *ARF4* genes. Proc. Natl. Acad. Sci. USA **102**: 9703-9708.

**Xia, R., Xu, J., Meyers, B.C.** 2017. The emergence, evolution, and diversification of the miR390-TAS3-ARF pathway in land plants. Plant Cell **29**: 1232-1247.

**Yan, J., Cai, X., Luo, J., Sato, S., Jiang, Q., Yang, J., Cao, X., Hu, X., Tabata, S., and Gresshoff, P.M., Luo, D.** (2010). The *REDUCED LEAFLET* genes encode key components of the trans-acting small interfering RNA pathway and regulate compound leaf and flower development in *Lotus japonicus*. Plant Physiol. **152**:797-807.

**Yifhar, T., Pekker, I., Peled, D., Friedlander, G., Pistunov, A., Sabban, M., Wachsman, G., Alvarez, J.P., Amsellem, Z., and Eshed, Y.** (2012). Failure of the tomato trans-acting short interfering RNA program to regulate *AUXIN RESPONSE FACTOR3* and *ARF4* underlies the *wiry* leaf syndrome. Plant Cell **24**:3575-3589.

**Yoshikawa, M., Peragine, A., Park, M.Y., Poethig, R.S.** 2005. A pathway for the biogenesis of trans-acting siRNAs in Arabidopsis. Genes Dev. **19:** 2164-2175.

**Yuan, Y.W.** (2019). Monkeyflowers (*Mimulus*): new model for plant developmental genetics and evo-devo. New Phytol. **222**: 694-700.

**Yuan, Y.-W., Sagawa, J.M., Young, R.C., Christensen, B.J., and Bradshaw, H.D.** (2013a). Genetic dissection of a major anthocyanin QTL contributing to pollinator-mediated reproductive isolation between sister species of *Mimulus*. Genetics **194**:255-263.

**Yuan, Y.-W., Sagawa, J.M., Di Stilio, V.S., and Bradshaw, H.D.** (2013b). Bulk segregant analysis of an induced floral mutant identifies a MIXTA-like R2R3 MYB controlling nectar guide formation in *Mimulus lewisii*. Genetics **194**: 523-528.

**Yuan, Y.-W., Sagawa, J.M., Frost, L., Vela, J.P., and Bradshaw Jr., H.D.** (2014). Transcriptional control of floral anthocyanin pigmentation in monkeyflowers (*Mimulus*). New Phytol. **204**:1013-1027.

**Zhong, J., Powell, S., and Preston, J.C.** (2016). Organ boundary NAC-domain transcription factors are implicated in the evolution of petal fusion. Plant Biol. **18**:893-902.

**Zhong, J., and Preston, J.C.** (2015). Bridging the gaps: evolution and development of perianth fusion. New Phytol. **208**:330-335.

**Zhou, C., Han, L., Fu, C., Wen, J., Cheng, X., Nakashima, J., Ma, J., Tang, Y., Tan, Y., and Tadege, M.** (2013). The trans-acting short interfering RNA3 pathway and no apical meristem antagonistically regulate leaf margin development and lateral organ separation,

as revealed by analysis of an *argonaute7/lobed leaflet1* mutant in *Medicago truncatula*. Plant Cell **25**:4845-4862.
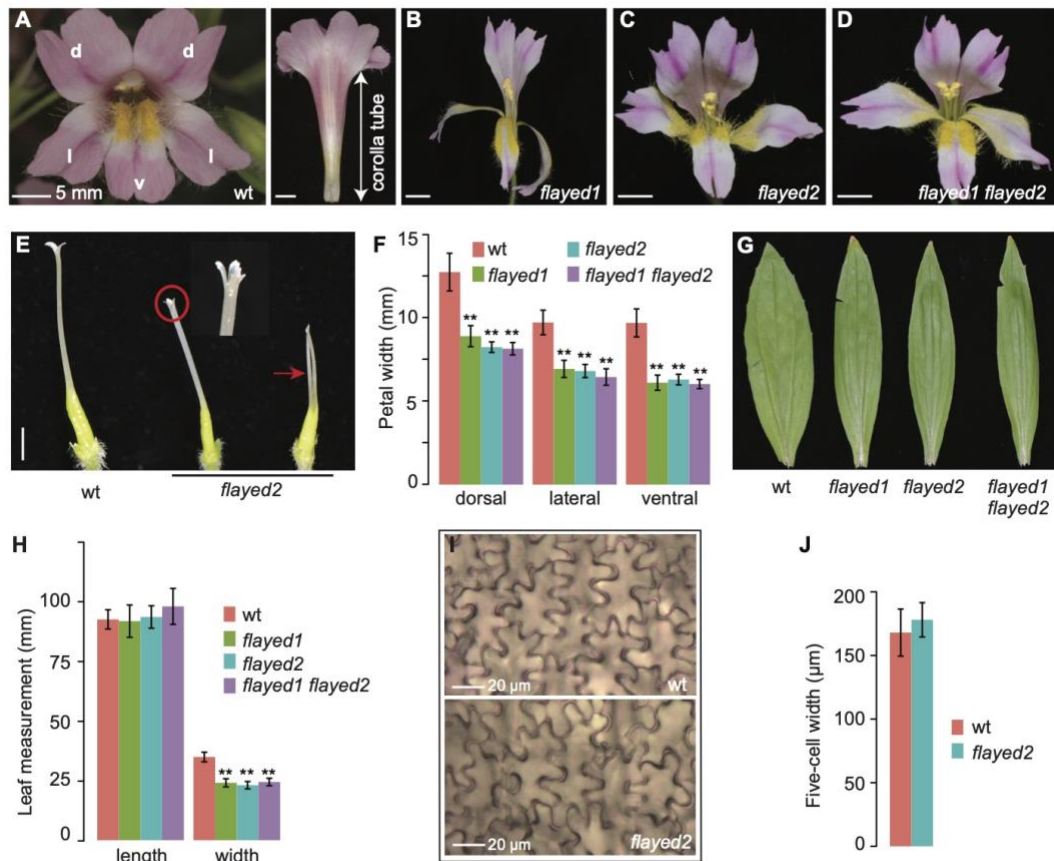
**Figure 1.** Phenotypic Characterization of the *flayed* Mutants.
(**A**) Face and side view of the wild-type *M. lewisii* (inbred line LF10) corolla. d: dorsal; l: lateral; v: ventral.
(**B**) Side view of *flayed1* corolla.
(**C and D**) Face view of *flayed2* (**C**) and the *flayed1 flayed2* double mutant (**D**).
(**E**) Pistil of the wild type (wt) and *flayed2*. The pistil phenotype of *flayed1* and the double mutant is the same as that of *flayed2*.
(**F**) Quantitative comparison of petal width in wt (n =18), *flayed1* (n = 10), *flayed2* (n = 12), and the double mutant (n = 12). Each flower was sampled from a distinct plant. Detailed measurement data are presented in Supplemental Table 1.
(**G**) Overall shape of the fourth leaf (the largest leaf) of mature plants.
(**H**) Quantitative comparison of length and width of the fourth leaf, with the same sample sizes as in (**F**). The leaf samples came from the same set of plants as in (**F**).
(**I**) Abaxial epidermal cells of dorsal petal lobes.
(**J**) Width of five contiguous abaxial epidermal cells of the dorsal petal lobes in the wt (n = 15) and *flayed2* (n = 15).
Scale bars in (**A-E**) are 5 mm. Error bars in (**F**), (**H**), and (**J**) are 1 SD. Asterisks indicate differences from the wild type (**$P < 0.01$, Student's *t* test), and the lack of asterisks indicates no significant difference from the wild type.
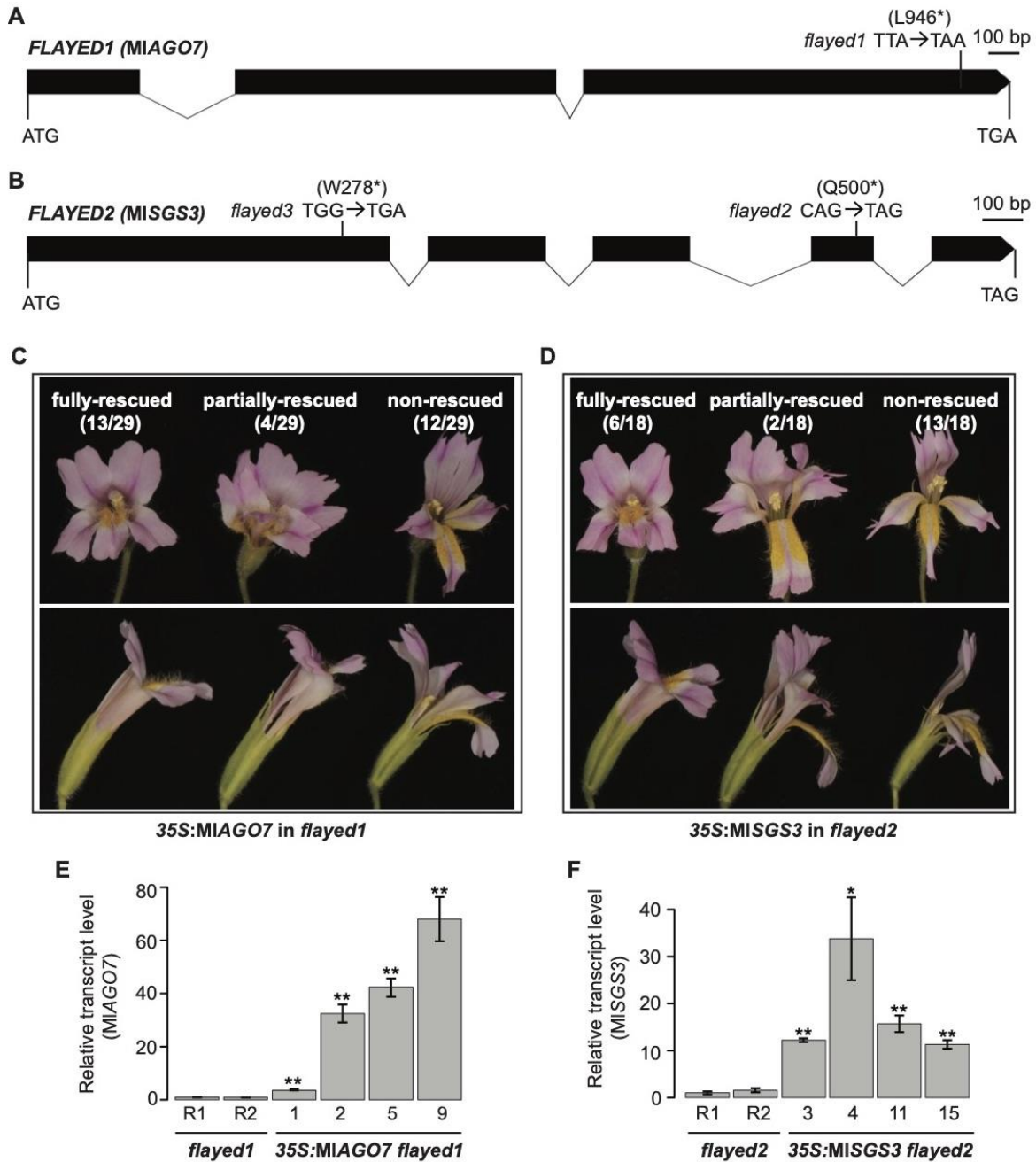
32

**Figure 2.** *FLAYED1* and *FLAYED2* Encode the Orthologs of Arabidopsis *AGO7* and *SGS3*.
(**A** and **B**) Schematics of Ml*AGO7* (**A**) and Ml*SGS3* (**B**) gene structure, with causal mutations indicated. Black box: exon; Line: intron. Scale bars are 100 bp.
(**C** and **D**) Flower phenotypes of *35Spro:MlAGO7* (**C**) and *35Spro:MlSGS3* (**D**) transgenics in the *flayed1* and *flayed2* mutant background, respectively (top: face view; bottom: side view). The proportion of fully-rescued, partially-rescued, and non-rescued lines are shown in parentheses.
(**E** and **F**) Relative transcript levels of Ml*AGO7* (**E**) and Ml*SGS3* (**F**) in 5 mm floral buds of four representative, fully rescued over-expression lines compared to the corresponding mutant backgrounds, as determined by RT-qPCR. Ml*UBC* was used as the reference gene. R1 and R2 represent two individual plants. Error bars represent 1 SD from three technical replicates. Asterisks indicate differences from the corresponding mutants (*$P < 0.05$, **$P < 0.01$, Student's *t* test).
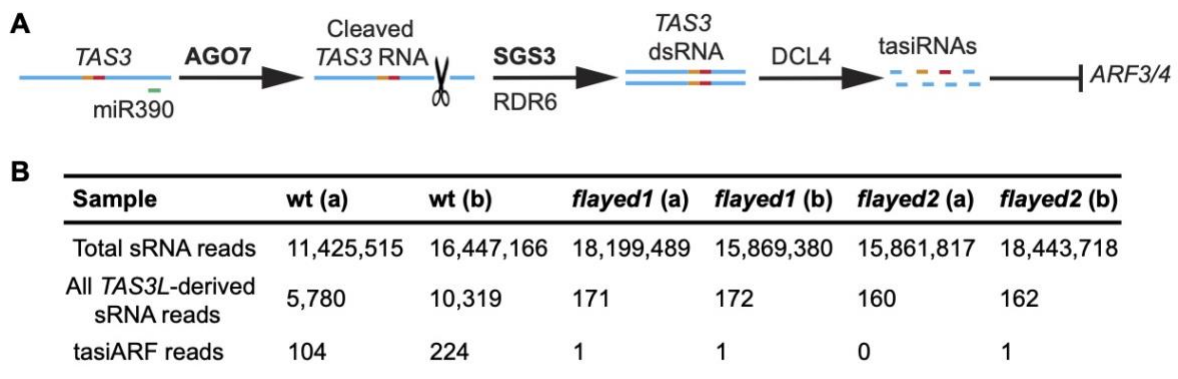

**A**

TAS3 → (AGO7) → Cleaved TAS3 RNA + miR390 → (SGS3, RDR6) → TAS3 dsRNA → (DCL4) → tasiRNAs ⊣ ARF3/4

**B**

| Sample | wt (a) | wt (b) | *flayed1* (a) | *flayed1* (b) | *flayed2* (a) | *flayed2* (b) |
|---|---|---|---|---|---|---|
| Total sRNA reads | 11,425,515 | 16,447,166 | 18,199,489 | 15,869,380 | 15,861,817 | 18,443,718 |
| All *TAS3L*-derived sRNA reads | 5,780 | 10,319 | 171 | 172 | 160 | 162 |
| tasiARF reads | 104 | 224 | 1 | 1 | 0 | 1 |

**Figure 3.** Small RNA Analysis.
(**A**) Schematic of the miR390-*TAS3-ARF* pathway. The orange and red lines represent the two tandem tasiARFs (see Supplemental Figure 1 for detailed annotations).
(**B**) Small RNA counts in the wild type (wt), *flayed1*, and *flayed2*. Two biological replicates were sequenced for each genotype. Each biological replicate consisted of pooled 5 mm floral buds from a distinct plant.

34
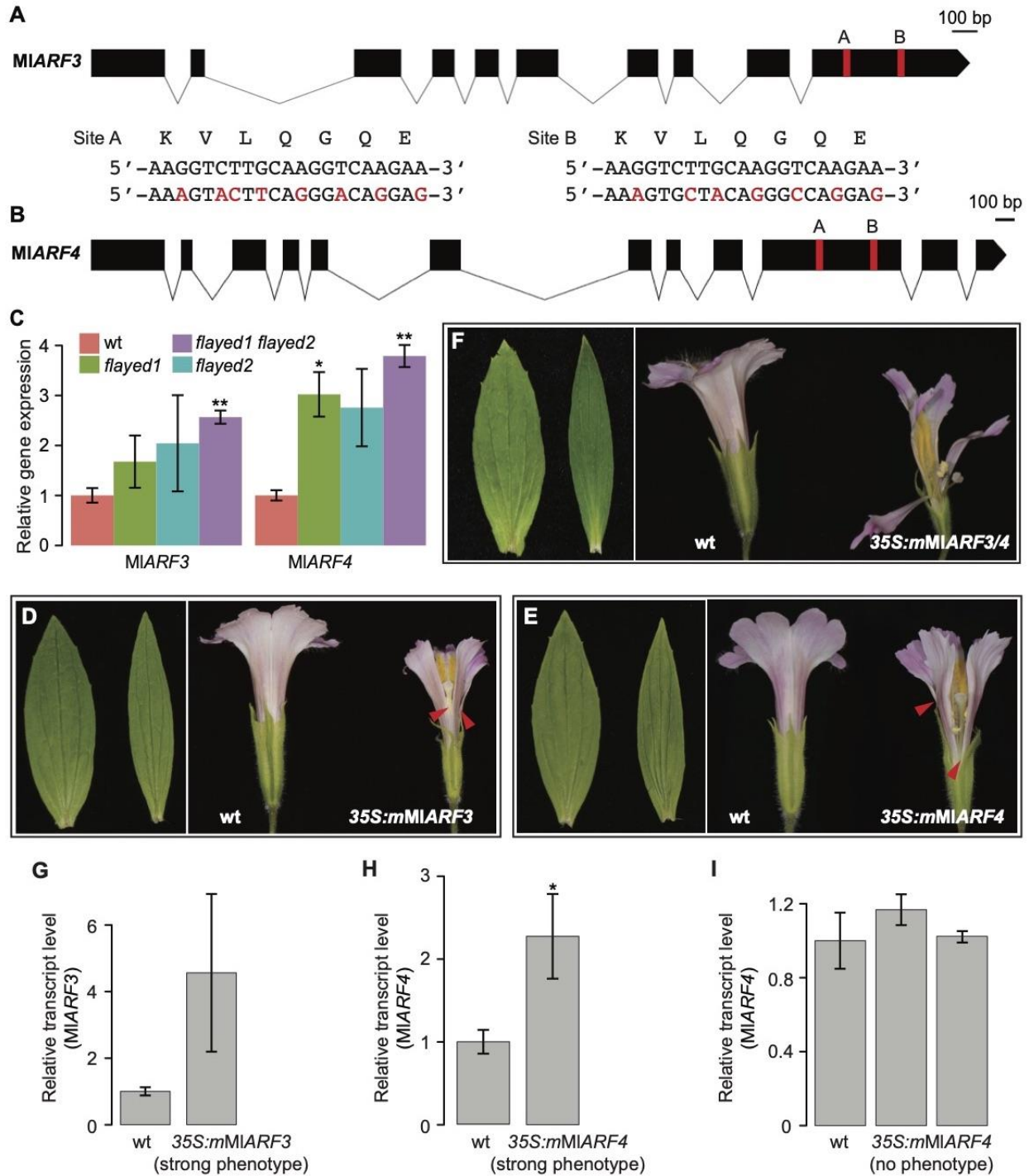
**Figure 4.** The *flayed1/2* Phenotypes are Primarily Mediated Through Up-regulation of MI*ARF3/4*.
(**A** and **B**) Schematics of MI*ARF3* (**A**) and MI*ARF4* (**B**) gene structure. Red bar: tasiARF binding site. Scale bars are 100 bp. The nucleotides highlighted in red are synonymous substitutions at the two tasiRNA binding sites that were introduced in the *35Spro:mMlARF3* and *35Spro:mMlARF4* constructs to circumvent tasiRNA repression.
(**C**) Relative transcript levels of MI*ARF3* and MI*ARF4* in 5 mm floral buds of mutant plants compared to the wild type (wt), as determined by RT-qPCR. MI*UBC* was used as the reference gene. Error bars represent 1 SD from three biological replicates (i.e., three individual plants) for each genotype.

(**D-F**) Leaf and flower phenotypes of the strongest *35Spro:mMlARF3* (**D**), *35Spro:mMlARF4* (**E**), and double transgenic line (**F**). Left: wt; right: transgenic line. The red arrow heads indicate points of petal separation.

(**G-I**) Relative transcript level of *MlARF3* in the *35Spro:mMlARF3* line with the strongest phenotype (**G**), *MlARF4* in the *35Spro:mMlARF4* line with the strongest phenotype (**H**), and *MlARF4* in two *35Spro:mMlARF4* transgenic lines without any obvious phenotypes (**I**). Ml*UBC* was used as the reference gene. Error bars represent 1 SD from three biological replicates (5 mm floral buds from three different plants for the wild type and from three lateral branches of the same $T_1$ plant for the transgenic lines).

Asterisks in the bar graphs (**C** and **G-I**) indicate differences from the wild type (*$P < 0.05$, **$P < 0.01$, Student's *t* test), and the lack of asterisks indicates no statistically significant difference from the wild type.
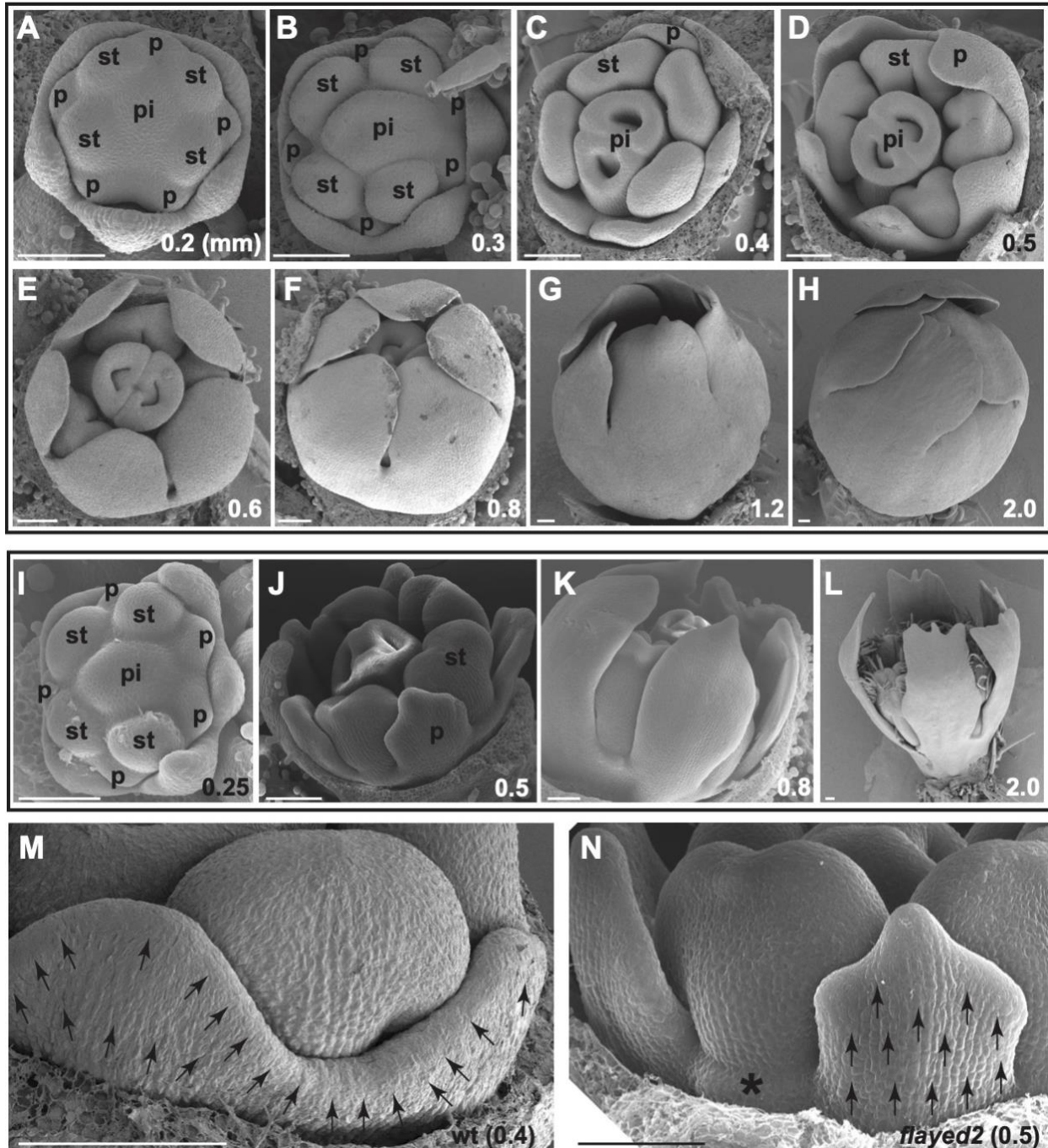
**Figure 5.** Scanning Electron Micrographs of *M. lewisii* Floral Development.
(**A-H**) Wild type LF10. The developmental stages are marked on the bottom right of each image by the diameter (in mm) of the corolla. From 0.4 mm onward, sepals were removed to show the petals.
(**I-L**) *flayed2*.
(**M** and **N**) Detailed view of two adjacent petal primordia and the inter-primordial region in the wild type (wt; 0.4 mm stage) (**M**) and *flayed2* (0.5 mm stage) (**N**). Arrows indicate growth directions, and the asterisk in (**N**) marks the arrested inter-primordial region.
Scale bars are 100 μm. p = petal; st = stamen; pi = pistil.
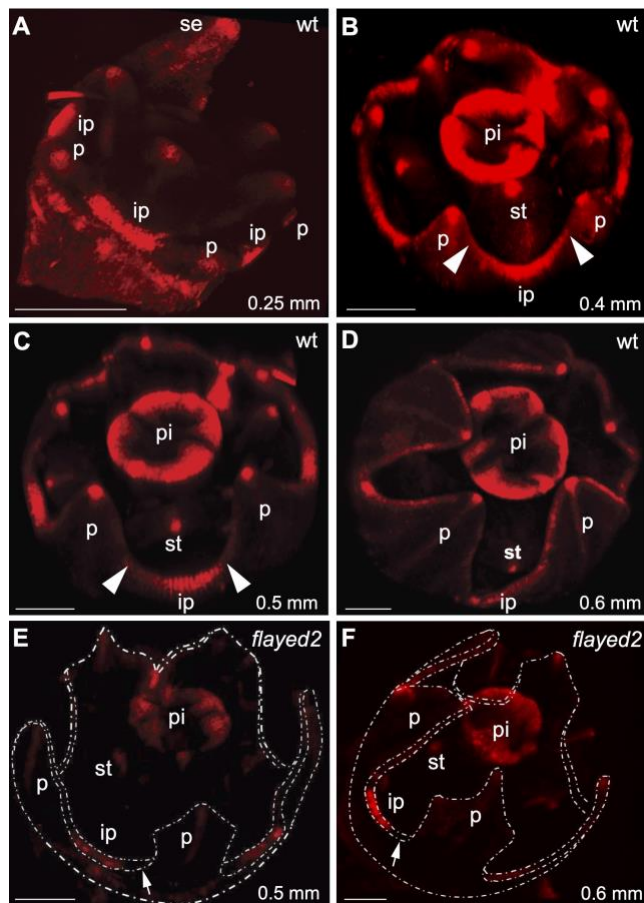
**Figure 6.** Patterns of Auxin Response in the Developing Corolla Buds of the Wild Type and *flayed2*, as Reflected by the *DR5rev:mRFPer* Reporter.

(**A-D**) Wild type (wt). The developmental stages are marked on the bottom right of each image by the diameter (in mm) of the corolla. The white arrow heads in (**B**) and (**C**) demarcate the synchronized growth zone encompassing the marginal meristematic cells at the base of the petal primordia and the inter-primordial cells. se = sepal; p = petal; ip = inter-primordial region; st = stamen; pi = pistil. Scale bars are 100 µm.

(**E** and **F**) *flayed2*. Shown in the same style as the wild type. The overall fluorescence signal is much weaker in the mutant compared to the wild type. Petal primordia and inter-primordial regions are outlined in white dashed lines. White arrows mark the gap at the junction between the petal primordium base and the inter-primordial region.
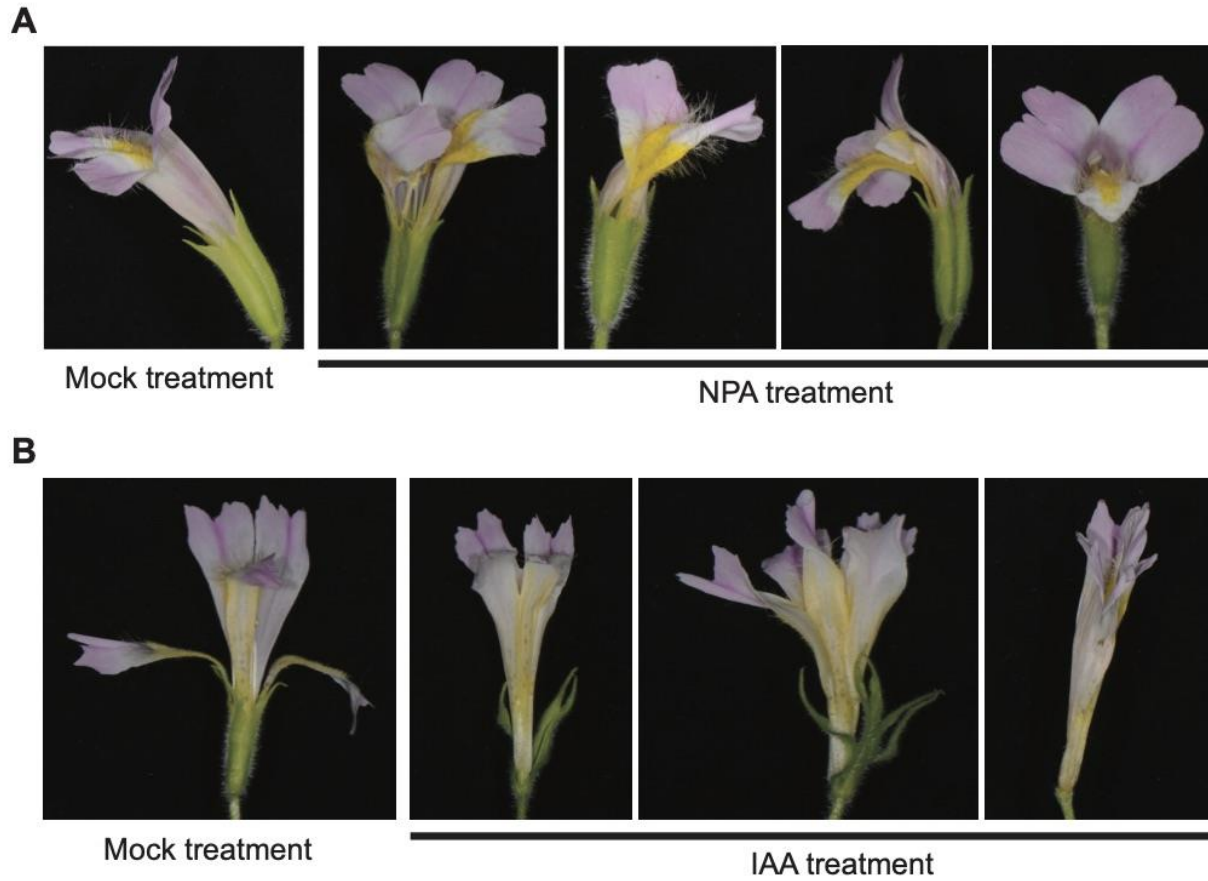
**Figure 7.** NPA and IAA Treatments.
(**A**) Exogenous application of 5 µM NPA to the apices of lateral shoots of the wild type *M. lewisii* resulted in various corolla tube defects in ~30% of the flowers.
(**B**) Exogenous application of 5 mM IAA to *flayed2* resulted in rescue of the corolla tube in 2% of the flowers.
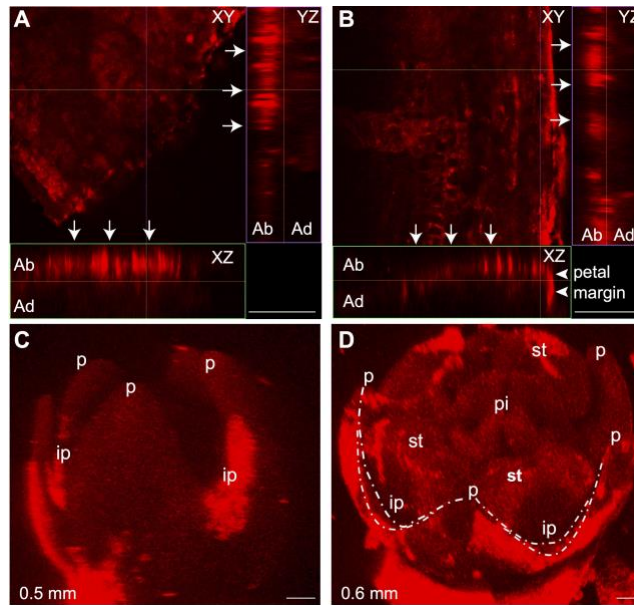
**Figure 8.** Ml*ARF4* Expression Pattern in Individual Petals and Flower Buds of Wild Type *M. lewisii*, as Revealed by the *ARF4pro:ARF4-RFP* Reporter.

**(A** and **B)** Confocal laser scanning microscopy of a single petal at the 3.0 mm corolla developmental stage. Representative orthogonal view of the Z-stack of an individual petal of *ARF4pro:ARF4-RFP* line 10 **(A)** and *ARF4pro:ARF4-RFP* line 7 **(B)**. Shown in the bottom green box and right purple box are single orthogonal sections of cross-sectional planes in XZ and YZ, respectively. The white arrows point to the abaxial side of the petal. Note that the cross-sectional XZ plane in **(B)** captured the petal margin (indicated by the arrowheads), where Ml*ARF4* is observed in both sides. Ad = Adaxial; Ab = Abaxial.

**(C** and **D)** Ml*ARF4* expression in whole flower buds; p = petal; ip = inter-primordial region; st = stamen; pi = pistil. Scale bars (bottom right corner of each panel) are 50 µm.
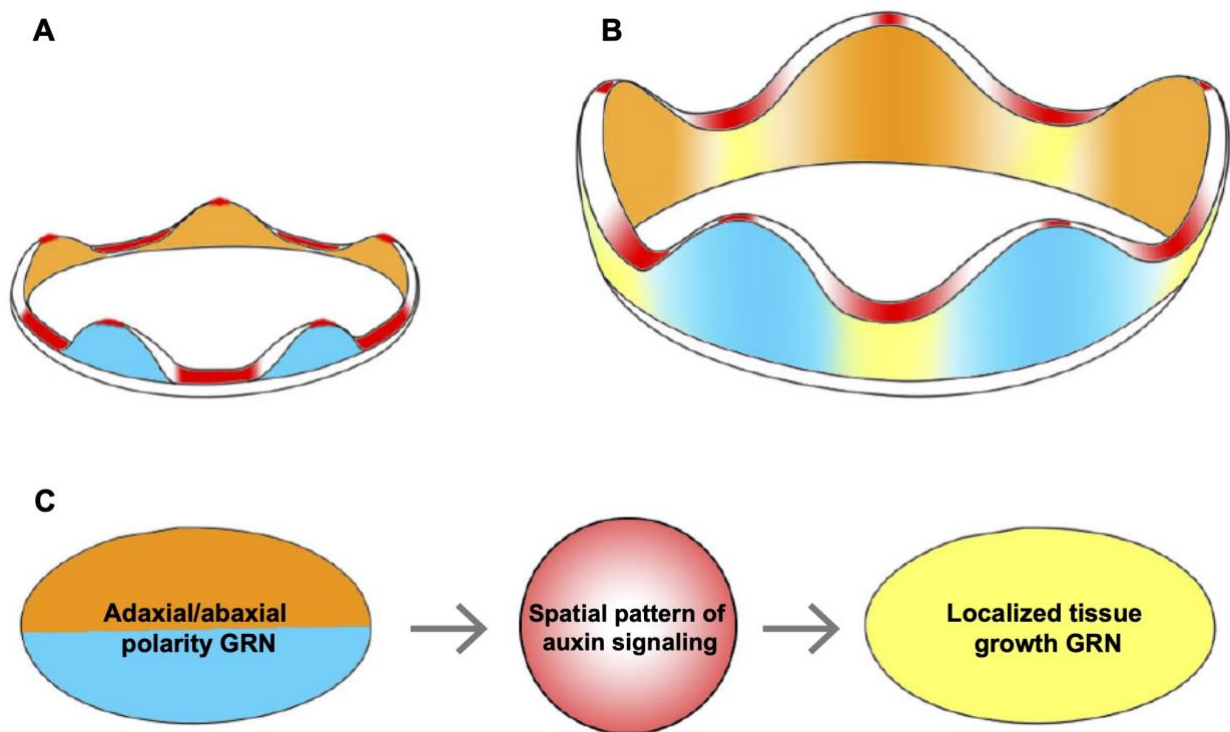
**Figure 9.** A Conceptual Model for the Developmental Genetic Control of Corolla Tube Formation in *Mimulus lewisii*.

(**A** and **B**) During phase I (**A**) auxin activity maxima promote initiation of individual petal primordia. During this phase there is also a broad zone of auxin response in the inter-primordial region, which leads to the initiation of upward growth around the entire circumference of the petal whorl and formation of the corolla tube during phase II (**B**). Blue and orange color indicates the abaxial and adaxial side of the petal, respectively. Yellow color indicates the inter-primordial zone.

(**C**) Genetic relationships among the three hypothetical modules. The delicate spatial pattern of auxin signaling plays a central role in directing the synchronized growth between the petal primordium base and the inter-primordial zone, and forms the core module of the model. The dynamics of auxin response in the developing corolla is at least partly regulated by the leaf adaxial/abaxial polarity network characterized in Arabidopsis. The downstream effector genes responsible for the auxin-induced localized tissue growth in the synchronized growth zone remain to be explored. GRN: Genetic Regulatory Network.

# Developmental Genetics of Corolla Tube Formation: Role of the tasiRNA-ARF Pathway and a Conceptual Model

Baoqing Ding, Rui Xia, Qiaoshan Lin, Vandana Gurung, Janelle M. Sagawa, Lauren E Stanley, Matthew Strobel, Pamela K. Diggle, Blake C. Meyers and Yao-Wu Yuan

This information is current as of September 12, 2020